Analysis of Thermally Diffused Single Mode Optical Fiber Couplers

by

Nirmalkumar Velayudhan

Thesis submitted to the Faculty of the

Virginia Polytechnic Institute and State University

in partial fulfillment of the requirements for the degree of

Master of Science

in

Electrical Engineering

APPROVED:

_____

Dr. Richard O. Claus, chairman

_____ _____

Dr. Kent A. Murphy Dr. Anbo Wang

February, 1997

Blacksburg, Virginia

Analysis of Thermally Diffused Single Mode Optical Fiber Couplers

by

Nirmalkumar Velayudhan

Richard O. Claus, Chairman

Electrical Engineering

Abstract

The phenomenon of dopant diffusion as a viable means of coupler fabrication is investigated. It is well known that the diffusion of dopants can improve the uniformity of multimode star couplers manufactured by the fused biconical taper technique. The theoretical basis for the same phenomenon in a single mode coupler is developed, on the basis of the theory of diffusion and the Gaussian approximation for circular fibers.

A novel technique to manufacture and design single mode optical fiber couplers with a minimization of the manufacturing complexity is demonstrated. Traditionally fused biconical tapered couplers have been manufactured by twisting, fusing and elongating optical fibers at elevated temperatures. Usually, high temperature oxy-hydrogen flames are used for such purposes and some degree of skill is needed for a human operator. The complexity of control procedures for automation of the process is greatly increased by the fact that the tapering process is an integral part of the feedback loop. This can be eliminated if a constant tension is maintained on the fibers in the heating process while heat is applied uniformly from a source such as a platinum wire furnace. Since the refractive index differentials responsible for the guiding phenomenon at optical frequencies are directly dependent on concentration of dopants like fluorine and germania, radial diffusion of such dopants causes the fiber cores that are heated in a platinum wire furnace to come closer together. Such proximity leads to the phenomenon of evanescent field interaction or coupling of optical power from one arm of the coupler to the other.

The time evolution of the coupling process can be predicted in theory. While initial results are promising, the ability to automate the manufacture of couplers will be successful only after greater control over the variables is established. It is the intention of this work to understand the physics behind the mechanism as well as to prove the feasibility of modeling real world phenomena under controlled conditions.

Acknowledgments

I would like to thank Professor Richard O. Claus for serving as my academic advisor, and providing me an invaluable opportunity to work with the Fiber and Electro-Optics Research Center (FEORC). I also want to thank my committee members, Dr. Kent Murphy and Dr. Anbo Wang for their corrections and suggestions for improving my thesis.

I am indebted to many FEORC staff and students for their support on this project. In particular, I would like to thank Mike Gunther for helping to conduct the measurements on the couplers. Special thanks go to Veeru Vuppala for his suggestions and support.

TABLE OF CONTENTS

1 Introduction

1.1 Dopant Diffusion as a Coupling Mechanism for Optical Fibers

Many different techniques are applied to the analysis of single mode couplers, and often a number of assumptions are made on the basis of the way the coupler is made. Bearing this in mind, a novel technique of coupler fabrication and design is suggested, albeit from a theoretical standpoint. While there is some limited experimental work included, this should be merely viewed as being proof of concept, with the idea that the practical issues raised may generate further attempts to improve the applicability of the present model.

The phenomenon of diffusion of typical optical fiber dopants like Germanium and Fluorine has been reported by many other workers [McL88, Bot88], the modeling of such phenomenon has been difficult, partially due to the intractability of the problem, as well as due to the lack of good characterization of the diffusion process. It has been demonstrated [McL88, Vup94] before that dopant diffusion can be held accountable for explanation of some of the various phenomena encountered in optical fiber couplers. [Vup94] reports the use of a dopant diffusion mechanism to improve the uniformity of large core multimode fiber couplers.

This work presents a study of the modeling of single mode couplers that are manufactured by dopant diffusion in a high temperature furnace. The assumption here is that the two fibers can be brought into close contact without significant tapering losses, i.e. the tapering is well within the adiabatic assumption for a single taper region. The fibers are then heated in a high temperature furnace with a constant temperature distribution over a length equal to 6 mm. Due to the heat applied, the dopant diffusion causes the cores to expand (in terms of the refractive index profiles), as well as decrease the refractive index delta, defined in any standard way. Accordingly, the evanescent field interaction causes a modal overlap phenomenon, whereby optical power is exchanged. Thus we see that traditional methods of analysis of Fused Biconical Taper (FBT) couplers [Bur88, Pay85] are not exactly applicable; rather the problem can be analyzed in terms of the crosstalk between two optical fibers as presented in [Sny83]. We neglect the modeling of losses, partly due to the problematic nature of the analysis, but also due to the experimental results that show negligible losses, in terms of industry accepted levels.

Chapters 2 and 3 treat the mathematical formalism involved in the model in rigorous detail; the purpose of this introduction is to present the concepts and justification for any assumptions made in our analysis. Firstly, as demonstrated in Chapter 2, solutions of the diffusion equation for a cylindrical optical fiber having a single dopant, either in the core or the cladding is presented. An approximately Gaussian dependence is noted, i.e. a bell shaped curve with a maximum and a smoothly decreasing amplitude is noted. Thus intuitively, we see that the Gaussian mode theory for circular optical fibers can be applied. As [Sny83] states, the Gaussian approximation for circular optical fibers is of particular interest to fibers that exhibit significant core/cladding dopant diffusion. Chapter 3 considers the mathematical derivation of the coupling phenomenon, using a linear superposition technique. It then goes on to explain mathematically the subtleties of the scalar wave equation and the weakly guiding condition. Finally, it ends with the derivation of the coupling coefficient for two parallel Gaussian index profile fibers. Chapter 4 is paramount to this thesis as the theoretical results developed in Chapters 2 and 3 are developed into two theoretical models, for the purposes of comparison. One model is an adaptation of work done by [Sny83, McL88], while the other is an extension of another model developed by [Sny83]. The two models work on two parallel sets of assumptions, and each of these is evaluated against a proof of concept experiment. The importance of the Gaussian approximation in the analysis is revealed by the results obtained. Chapter 5 presents the conclusions and directions for future work.

2 The Problem of Diffusion

2.1 Introduction

In simplistic terms, the process of diffusion is a mass transport mechanism whereby a substance moves from a region of higher concentration to a region of lower concentration. This process is usually defined in terms of differential equations that account for the many variables involved in the process. The fundamental properties of diffusion are described by Ficks' Laws. We do not intend to explore the derivation of these results at this level, but apply them along the lines suggested by [Cra75] and treat the problem of dopant diffusion in a cylindrical optical fiber from a mathematical standpoint. However, the intuitive basis for the form of the solution will be developed, to gain insight into the mechanism. Note that diffusion at the molecular level is not considered.

2.2 Diffusion in Homogenous Media

In vector analytic terms the diffusion equations can be expressed for any coordinate system can be expressed as

$$\frac{\partial C}{\partial t} = \nabla \bullet (\mathbf{D} \times \mathbf{C}) \ . \qquad \text{(EQ 2.2-1)}$$

In cylindrical coordinates where the parameters of interest are r, θ, and z defined in the usual manner, equation (2.2-1) reduces to

$$\frac{\partial \mathbf{C}}{\partial \mathbf{t}} = \frac{1}{r}\left\{\frac{\partial}{\partial r}\left(rD\frac{\partial C}{\partial t}\right) + \frac{\partial}{\partial \theta}\left(\frac{D}{r}\frac{\partial C}{\partial \theta}\right) + \frac{\partial}{\partial z}\left(rD\frac{\partial C}{\partial z}\right)\right\}, \qquad \text{(EQ 2.2-2)}$$

where D is the diffusion coefficient having the dimensions L^2T^{-1}, and C is the concentration of the substance undergoing diffusion, defined in any standard way. We consider the problem of diffusion in a cylinder from first principles, by regarding the issue of diffusion in one dimension, for a constant value of D. A fundamental assumption in the analysis is that the value of D remains a constant for a fixed temperature. Equation (2.2-1) reduces to

$$\frac{\partial C}{\partial t} = D\frac{\partial^2 C}{\partial x^2}, \qquad \text{(EQ 2.2-3)}$$

and the solution to this is of the form

$$C = \frac{A}{\sqrt{t}} exp\left(\frac{x^2}{4Dt}\right). \qquad \text{(EQ 2.2-4)}$$

Note the symmetrical nature of the solution about the *x*-axis at *x=0*. For *t=0*, it vanishes everywhere except at *x=0*, where it becomes infinite and assumes the form of a delta function. It is also important to note the principle of *superposition and reflection* at a boundary. For instance, consider the case of a semi-infinite medium, extending as a cylinder (remember that the initial distribution was a delta function) with an impermeable boundary at *x=0*. The solution for *x<0* can be reflected and added to the solution for diffusion in the *x>0* region. This is done as the equation itself is linear, and hence the sum of the solutions is in itself a solution to the diffusion equation. To examine the problem of a finite source width we initially consider the one-dimensional case, i.e. the boundaries at *t=0*, which may be defined as:

$$C = C_0, \qquad x < 0$$

$$C = 0, \qquad x > 0. \qquad \text{(EQ 2.2-5)}$$

As an example [Cra75] considers the case of a long column of clear water resting on a long column of solution, or two metal bars placed end to end. The solution is gleaned by considering the extended distribution (for *x<0* from equation (2.2-5)) to be composed of an infinitum of line sources and applying the principle of superposition to the infinitum of corresponding solutions.

This is illustrated in Fig. (2.2-1) where the concentration *C* at point *p*, a distance ξ from a narrow strip source of width $\delta\xi$ is given by

$$C(x, t) = \frac{C_0 \delta\xi}{2\sqrt{\pi Dt}} exp\left(-\frac{\xi^2}{4Dt}\right). \qquad \text{(EQ 2.2-6)}$$

The quantity $C_0\delta\xi$ denotes the amount of substance diffusing in a cylinder of infinite length and unit cross section. Thus by integration over all such elements $\delta\xi$ we may find the concentration as a function of distance and time, i.e.,

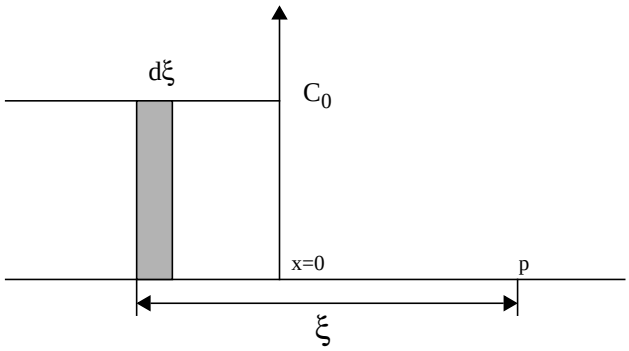

FIGURE 2.2-1 Framework for modeling the superposition principle.

$$C(x,t) = \int_{x}^{\infty} \frac{C_0 \delta\xi}{2\sqrt{\pi D t}} exp\left(-\frac{\xi^2}{4Dt}\right) d\xi \ . \qquad \text{(EQ 2.2-7)}$$

Note that a dummy variable, say *A* where

$$A = \frac{\xi}{2\sqrt{Dt}} \qquad \text{(EQ 2.2-8)}$$

and

$$dA = \frac{d\xi}{2\sqrt{Dt}} \qquad \text{(EQ 2.2-9)}$$

is used. Making the necessary change in variables and the change in limits,

$$C(x,t) = \frac{C_0}{\sqrt{\pi}} \int_{x/(2\sqrt{Dt})}^{\infty} exp(-A^2) dA \ . \qquad \text{(EQ 2.2-10)}$$

This can be defined in terms of the complementary error function *erfc(A)*. We know that

$$erfc(z) = \frac{2}{\sqrt{\pi}} \int_{z}^{\infty} exp(-\eta^2) d\eta \ . \qquad \text{(EQ 2.2-11)}$$

The error function and the complementary error function are a well tabulated series of integrals [Abr70]. Thus

$$C(x,t) = \frac{C_0}{2} erfc\left(\frac{x}{2\sqrt{Dt}}\right). \qquad \text{(EQ 2.2-12)}$$

Let us examine the diffusion of a substance that initially has a step distribution in a region of width *2h*. The region of integration is modified from *[x,∞]* to *[x-h,x+h]*, i.e.

$$C(x,t) = \frac{C_0}{2\sqrt{\pi Dt}} \int_{x-h}^{x+h} exp\left(-\frac{\xi^2}{4Dt}\right) d\xi \ . \qquad \text{(EQ 2.2-13)}$$

Applying the usual change in variables as stated before in equations (2.2-8) and (2.2-9), this reduces to

$$C(x,t) = \frac{C_0}{2}\left\{ erf\left[\frac{h-x}{2\sqrt{Dt}}\right] + erf\left[\frac{h+x}{2\sqrt{Dt}}\right]\right\}. \qquad \text{(EQ 2.2-14)}$$

Since the system is symmetrical, the system can be cut in half by a plane at *x=0*, without affecting the distribution. Thus we can consider the semi-infinite problem, with the boundary at *x=0*, and the application of superposition.To examine the general philosophy of having an impermeable boundary, we consider the case of the following boundary condition:

$$\frac{\partial C}{\partial x} = 0, \qquad x = 1. \qquad \text{(EQ 2.2-15)}$$

Thus reflection takes place at the boundaries *x=0* and *x=l* an infinite number of times. The original solution given by equation (2.2-14) corresponds to two error functions. The solution for an infinite number of reflections may thus be constructed by an infinite sum of such functions, i.e.

$$C = \frac{C_0}{2}\left\{ erf\left[\frac{h-x}{2\sqrt{Dt}}\right] + erf\left[\frac{h+x}{2\sqrt{Dt}}\right] + erf\left[\frac{(2l+h)-x}{2\sqrt{Dt}}\right] + \right.$$

$$\left. erf\left[\frac{(2l+h)+x}{2\sqrt{Dt}}\right] + erf\left[\frac{-(2l-h)-x}{2\sqrt{Dt}}\right] + erf\left[\frac{-(2l-h)+x}{2\sqrt{Dt}}\right] + \ldots \right\} \qquad \text{(EQ 2.2-16)}$$

Rewriting in terms of error functions summed to infinity,

$$C(x,t) = \frac{C_0}{2}\sum_{n=-\infty}^{\infty}\left\{erf\left(\frac{h-2nl+x}{2\sqrt{Dt}}\right)+erf\left(\frac{h+2nl-x}{2\sqrt{Dt}}\right)\right\} . \qquad \text{(EQ 2.2-17)}$$

Thus we see a simplified explanation of the typical form of solution for the diffusion equation. The use of the one dimensional case merely serves to gain insight into the mathematical formalism. The solution that is of interest to us is by the nature of the problem most suited to the cylindrical coordinate system. This therefore does turn out to be a form of Bessel's differential equation, familiar to waveguide theoreticians and many other branches of science and engineering. The equations are set up in terms of theory worked out in [Car59] and are based on results shown in [Cra75]. We accordingly present the solution of [Cra75] and see how they are applicable to the case of Fluorine doped step index fibers as well as Germania doped step index fibers.

2.3 Diffusion in a Cylindrical Doped Dielectric Waveguide

For an impermeable surface condition with an initial concentration distribution *f(r),*

$$C = \frac{2}{b^2}\left(\int_0^b r' f(r')dr' + \sum_{n=1}^{\infty} exp(-D\alpha_n^2 t)\times\frac{J_0(r\alpha_n)}{J_0^2(b\alpha_n)}\int_0^b r' f(r')J_0(\alpha_n r')dr'\right), \qquad \text{(EQ 2.3-1)}$$

where α_n represents the roots of

$$J_1(b\alpha_n) = 0 . \qquad \text{(EQ 2.3-2)}$$

Let *b* represent the cladding radius for a step index fiber and *a* be the core radius. The diffusion coefficient is *D, r* is the radius and *t* is the time of heating. Therefore the initial conditions can be represented as

$$f(r') = C_0, \qquad 0 \le r < a$$

$$f(r') = 0, \qquad a \le r < b . \qquad \text{(EQ 2.3-3)}$$

Substituting in equation (2.3-1) we get

$$C = \frac{a^2}{b^2}C_0 + \frac{2aC_0}{b^2}\sum_{n=1}^{\infty} exp(-D\alpha_n^2 t) \times \frac{J_0(r\alpha_n)}{\alpha_n J_0^2(b\alpha_n)} \cdot J_1(a\alpha_n) \quad , \qquad \text{(EQ 2.3-4)}$$

where the relationship for the indefinite integral of the Bessel function of the first kind of order 0 is

$$\int zJ_0(az)dz = \frac{z}{a}J_1(az) \ . \qquad \text{(EQ 2.3-5)}$$

Now consider the case for a Fluorine doped fiber having a step profile. The new initial conditions are given by

$$f(r') = 0, \qquad 0 \le r < a$$

$$f(r') = C_0, \qquad a \le r < b. \qquad \text{(EQ 2.3-6)}$$

This result when substituted into equation (2.3-1) leads to the following solution for the concentration *C*:

$$C = \frac{C_0(b^2 - a^2)}{b^2} - \frac{2aC_0}{b^2}\sum_{n=1}^{\infty} exp(-D\alpha_n^2 t) \cdot \frac{J_0(r\alpha_n)}{\alpha_n J_0^2(b\alpha_n)} \cdot J_1(a\alpha_n) \quad . \qquad \text{(EQ 2.3-7)}$$

3 The Problem of Coupling

3.1 Modeling the Coupling Behavior

The approach taken in the following analysis is an application of results presented in [Sny83] with a comparison of the results of an exact analysis of the mode coupling problem with a Gaussian best fit. The analytical model closely mimics that presented in [Sny83] and the model is extended using the diffusion model shown in Chapter 2. Note that the use of the word exact is questionable, but the gain in the tractability of the problem far outweighs any error introduced by the approximation. As stated earlier, the problem is considered as crosstalk between two optical fibers whose mode field radii are broadened by diffusion. Thus there is an interaction between the fields of the two fibers and optical power is exchanged between the two fibers. One fiber can be regarded as the perturbed fiber (i.e. the fiber into which no optical power is launched) and the second can be regarded as the perturbing fiber into which optical power is launched. The ray analysis approach treats the problem as one of evanescent field interaction, i.e. frustrated total internal reflection or tunneling. This approach is particularly useful to our analysis as the phenomenon of crosstalk between two parallel identical fibers can be used, since the underlying assumption is that there is no z dependent non-uniformity in the region of interest. This proceeds from the analysis of diffusion in the earlier chapter on diffusion, where the assumption was made that diffusion from the fibers is purely radial.

3.2 Crosstalk

Two caveats must be borne in mind; that the analysis is correct only under the weakly guiding assumption and that the optical separation is sufficient to ensure that superposition of the modal fields is valid. Consider two fibers that are in proximity to each other as indicated in Fig (3.2-1). We restrict the analysis to the case of *2x2* couplers that are single moded at the wavelength of interest when considered in isolation. Coupling can be represented by two coupled differential equations. The field solutions are constructed from solutions to the scalar wave equation, and thus the polarization of the field is not accounted for in the strict analysis. The scalar wave equation can be represented as:

$$\nabla_t^2 \Psi + (k_0^2 n^2 - \beta^2)\Psi = 0 , \qquad \text{(EQ 3.2-1)}$$

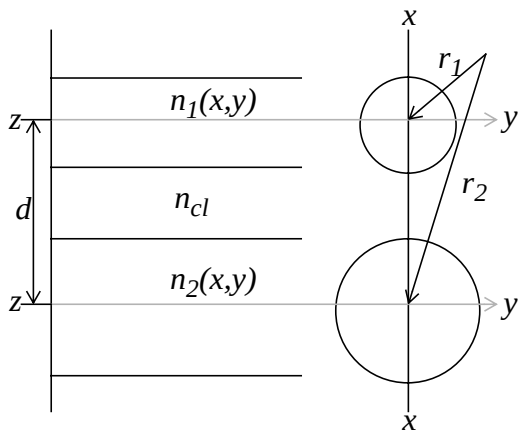

FIGURE 3.2-1 Coordinate System for Crosstalk Analysis

where Ψ is a field solution in any Cartesian coordinate of **E** or **H** representable in the standard cylindrical coordinate system. k_0 is the free space wave number, n the refractive index in the region of interest which for the case of the index profiles under consideration is symmetrical about the z axis, and a function of the radial coordinate r. β is the propagation constant. The expressions for the **E** field may then be reduced to:

$$E_{x1}(x,y,z) = a_1(z)\Psi_1(x,y)exp(-j\beta z)/\sqrt{N_1} = b_1(z)\Psi_1(x,y)/\sqrt{N_1} \qquad \text{(EQ 3.2-2)}$$

and

$$E_{x2}(x,y,z) = a_2(z)\Psi_2(x,y)exp(-j\beta z)/\sqrt{N_2} = b_2(z)\Psi_2(x,y)/\sqrt{N_2}, \qquad \text{(EQ 3.2-3)}$$

where the *a's* and *b's* represent the modal amplitude coefficients. Note the explicit *z* dependence of the amplitude coefficients. The factors N_1 and N_2 are normalization parameters that arise from the process of treating these as orthonormal modes. These may be represented generically as:

$$N = \frac{n_{co}}{2}\sqrt{\frac{\varepsilon_0}{\mu_0}}\int_{A_\infty}\Psi^2 dA, \qquad \text{(EQ 3.2-4)}$$

where n_{co} denotes the core index of refraction. The overall region of integration is represented by the area A_∞ where the cladding is assumed to extend to infinity. It can be shown that the coupled integro-differential equation that represents the process of treating one fiber as a perturbation of the other is:

$$\frac{db_1}{dz} - j\beta_1 b_1 = \frac{jk}{4}\sqrt{\frac{\varepsilon_0}{N_1\mu_0}}\int_{A_\infty}(n^2 - \bar{n}_1^2)\Psi\bar{\Psi}_1 dA. \qquad \text{(EQ 3.2-5)}$$

For a strict analysis the infinite set of radiation modes and the finite set of guided modes have to be considered. This would mean solving the expression for the scalar field for a large number of modes and thus having a large number of coupled equations. In order to simplify the problem the principle of superposition can be applied under the approximation that the fields in the fiber are a linear sum of the field of the individual fibers in isolation. This approximation of course assumes that the fibers are not too close to each other optically, and that they are very similar, if not identical. Thus we can approximate the total field for the waveguide by the expression

$$\Psi(x,y,z) = b_1(z)\Psi_1(x,y)/\sqrt{N_1} + b_2(z)\Psi_2(x,y)/\sqrt{N_2}. \qquad \text{(EQ 3.2-6)}$$

This when substituted into equation (3.2-5) gives the result

$$\frac{db_1}{dz} - j(\beta_1 + C_{11})b_1 = jC_{12}b_2. \quad \text{(EQ 3.2-7)}$$

Similarly, we treat the first fiber as being perturbed by the presence of the second fiber, and obtain

$$\frac{db_2}{dz} - j(\beta_2 + C_{22})b_2 = jC_{21}b_1. \quad \text{(EQ 3.2-8)}$$

Equation (3.2-8) may be obtained by duality also from equation (3.2-7). The C_{lm} coefficients are the coupling coefficients defined as

$$C_{lm} = \frac{k}{4}\sqrt{\frac{\varepsilon_0}{N_i N_j \mu_0}} \int_{A_\infty} (n^2 - n_1^2)\Psi_l \Psi_m dA, \quad \text{(EQ 3.2-9)}$$

where *l,m=1,2*. Further approximations may be made to this by considering the fact that over the core of fiber *l*, the field solution due to fiber *m* decays exponentially and thus C_{12} and C_{21} are negligible in comparison with the β_1 and β_2 terms respectively. Under the weakly guiding approximation [Saf93], we know that the allowed value for β is

$$k_0 n_{cl} < \beta < k_0 n_{co} \quad \text{(EQ 3.2-10)}$$

and hence the self coupling coefficients C_{11} and C_{22} are negligible.

A striking feature of modeling the crosstalk between fibers that are identical or very nearly so is that under resonant conditions, total power transfer can occur between the two fibers. If this condition is not met, then the effect of coupling to backward propagating modes as well as to radiation modes must be included and the modeling of this phenomenon becomes difficult. Accordingly, the resonance condition means that the cross coupling coefficients are identical, i.e.,

$$C_{12} \cong C_{21} = C \cong \frac{k}{4}\sqrt{\frac{\varepsilon_0}{N_1 \mu_0}} \int_{A_\infty} (n^2 - \bar{n}^2)\Psi_1 \Psi_2 dA, \quad \text{(EQ 3.2-11)}$$

from equation (3.2-9). This when substituted into equations (3.2-7) and (3.2-8) gives rise to the following result for the condition that when *z=0* the amplitude coefficients are $b_1(z)=b_1(0)$ and $b_2(z)=b_2(0)$:

$$b_1(z) = \{ \quad b_1(0)\cos\left(\frac{C}{M}z\right) + \qquad \text{(EQ 3.2-12)}$$

$$jM\left[b_2(0) + \frac{\bar{\beta}_1 - \bar{\beta}_2}{2C}b_1(0)\right]\sin\left(\frac{C}{M}z\right)\Big\}exp(j\bar{\beta}z)$$

and

$$b_2(z) = \{ \quad b_2(0)\cos\left(\frac{C}{M}z\right) + \qquad \text{(EQ 3.2-13)}$$

$$jM\left[b_1(0) + \frac{\bar{\beta}_1 - \bar{\beta}_2}{2C}b_2(0)\right]\sin\left(\frac{C}{M}z\right)\Big\}exp(j\bar{\beta}z) \quad ,$$

where

$$\bar{\beta} = \frac{\beta_1 + \beta_2}{2}, \qquad \text{(EQ 3.2-14)}$$

and

$$M = \left[1 + \frac{(\bar{\beta}_1 - \bar{\beta}_2)^2}{4C^2}\right]^{-1/2} . \qquad \text{(EQ 3.2-15)}$$

Thus we see that the modal amplitudes show a sinusoidal dependence along the z dimension. To examine the power flow along the composite waveguide, we consider the intensity distribution as the magnitude of the time averaged Poynting vector. The field representation of any parameter of interest can be represented as

$$E_1(x, y, z) = e_1(x, y)exp(-j\beta_1 z) \qquad \text{(EQ 3.2-16)}$$

$$= [e_{tj}(x, y) + e_{zj}(x, y)\bar{z}]exp(-j\beta z)$$

and

$$H_1(x, y, z) = h_1(x, y)exp(-j\beta_1 z) \qquad \text{(EQ 3.2-17)}$$

$$= [h_{tj}(x, y) + h_{zj}(x, y)\bar{z}]exp(-j\beta z) .$$

The value of the propagation constant β is unique for each mode. For a nonabsorbing waveguide, which is a reasonable approximation for an optical fiber, power flows along the axis of the waveguide, i.e. along the *z* dimension. The time averaged Poynting vector is then given by

$$S_1 = \frac{|a_1|^2}{2} Re\{E_1 \times H_j^* \cdot \bar{z}\} = \frac{|a_1|^2}{2} e_1 \times h_1^* \cdot \bar{z}, \qquad \text{(EQ 3.2-18)}$$

where S_1 is the intensity or optical power. Note that for convenience the transverse field components are considered to be real and accounting for the normalization, from equation (3.2-18) and equations (3.2-2) and (3.2-3), we see that the power in each corresponding mode is

$$P_1(z) = |b_1(z)|^2 \qquad \text{(EQ 3.2-19)}$$

and

$$P_2(z) = |b_2(z)|^2. \qquad \text{(EQ 3.2-20)}$$

The quantities $b_1(z)$ and $b_2(z)$ from equations (3.2-12) and (3.2-13) when substituted into equations (3.2-19) and (3.2-20) give rise to the following equations:

$$P_1(z) = P_1(0) + M^2\{P_2(0) - P_1(0) + \frac{\bar{\beta}_1 - \bar{\beta}_2}{C}\sqrt{P_1(0)P_2(0)}\}\sin^2\left(\frac{C}{M}z\right) \qquad \text{(EQ 3.2-21)}$$

and

$$P_2(z) = P_2(0) + M^2\{P_1(0) - P_2(0) - \frac{\bar{\beta}_1 - \bar{\beta}_2}{C}\sqrt{P_1(0)P_2(0)}\}\sin^2\left(\frac{C}{M}z\right). \qquad \text{(EQ 3.2-22)}$$

Again, the assumption of real values for the modal parameters ensures that the modes are in phase at *z=0*. The condition that initially power is launched into one fiber and initially this fiber contains all the power at *z=0* may be enforced, i.e.

$$P_1(0) = 1 \qquad \text{(EQ 3.2-23)}$$

and

$$P_2(0) = 0. \quad \text{(EQ 3.2-24)}$$

This leads to the result [McI73]:

$$P_1(z) = 1 - M^2 \sin^2\left(\frac{C}{M}z\right) \quad \text{(EQ 3.2-25)}$$

and

$$P_2(z) = M^2 \sin^2\left(\frac{C}{M}z\right). \quad \text{(EQ 3.2-26)}$$

From these equations it becomes obvious that a portion M^2 of the power in the first fiber is transferred to the second fiber and back. This occurs spatially along the z direction and for identical fibers complete power transfer occurs in one beat length z_b defined as

$$z_b = \frac{2\pi M}{C}. \quad \text{(EQ 3.2-27)}$$

The representation of the fields as a linear combination of the fields of the individual fibers is valid under the condition that the fibers are similar and optically well separated. Examination of equation (3.2-15) reveals the reason why coupling under these conditions would be negligible for significantly different fibers. The coupling coefficient C is small with regard to β_1 and β_2 and therefore as it appears in the denominator of the term containing β_1, β_2 and C, it is of significant magnitude to cause the value of M to be very small. We see therefore that the coupling as defined by equations (3.2-25) and (3.2-26) becomes negligible for non-identical fibers.

3.3 The Gaussian Approximation for Circular Fibers

3.3.1 The Scalar Wave Equation and Weakly Guiding Waveguides

In this section we consider the theoretical implications of modeling the diffused profiles under the Gaussian approximation followed by [Sny81]. At this juncture it is well worth commenting on the various possibilities open in terms of analytic techniques. While

this enumeration is by no means exhaustive, it covers the salient and feasible techniques that could be used. The fundamental assumptions in the consideration of most dielectric waveguides of practical interest are that they are nonabsorbing and generally translational invariant, i.e., there is no *z*-dependent non-uniformity. While this is strictly not true for fused couplers, especially the biconical tapered variety, for a diffused coupler, we make the translational invariance approximation. This of course neglects the change in the fiber dimension after diffusion broadening of the core, but we model this as an step transition in the cores. Modeling of the loss on the basis of a modal overlap formalism in electromagnetic theory has not been generally successful, and is further disregarded.

Therefore, before we detail the various approximations under the Gaussian approximation for circular fibers, it is instructive to examine the vector wave equation and the issue of polarization. The field solution for a time harmonic electromagnetic field is of the form expressed in equations (3.2-16) and (3.2-17), where propagation is defined in the *z* direction. Note that the time dependency has been suppressed. Normally the explicit *z*-dependence is also suppressed. Also note that the system assumed here is Cartesian, and a mode is a field solution that does not change in the transverse direction as the wave travels in the *z* direction [Saf93].

By elimination of either the **E** or **H** fields from Maxwell's equations the inhomogenous vector wave equations are obtained, i.e.

$$(\nabla^2 + n^2k^2)E = -\nabla(E_t \cdot \nabla_t ln(n^2)) - j\sqrt{\frac{\varepsilon_0}{\mu_0}}\left\{kJ + \frac{1}{k}\nabla\left(\frac{\nabla \cdot J}{n^2}\right)\right\} \qquad \text{(EQ 3.3-1)}$$

and

$$(\nabla^2 + n^2k^2)H = (\nabla\times H)\times\nabla_t ln(n^2) - \nabla\times J - J\times\nabla_t ln(n^2)\,. \qquad \text{(EQ 3.3-2)}$$

We refresh the following mathematical identities to provide crucial background information. In Cartesian coordinates

$$\nabla\Psi = \frac{\partial\Psi}{\partial x}\bar{x} + \frac{\partial\Psi}{\partial y}\bar{y} + \frac{\partial\Psi}{\partial z}\bar{z} = \nabla_t\Psi + \frac{\partial\Psi}{\partial z}\bar{z}\,, \qquad \text{(EQ 3.3-3)}$$

where Ψ is a scalar quantity. For a vector A, with Cartesian coordinates A_x, A_y, and A_z,

$$\nabla \cdot A = \frac{\partial A_x}{\partial x} + \frac{\partial A_y}{\partial y} + \frac{\partial A_z}{\partial z} = \nabla_t \cdot A_t + \frac{\partial A_z}{\partial z} \quad \text{(EQ 3.3-4)}$$

and

$$\nabla^2 A = \nabla(\nabla \cdot A) - \nabla\times(\nabla\times A)\,. \quad \text{(EQ 3.3-5)}$$

It is worthwhile pointing out that the above equation applies for an arbitrary coordinate system. In Cartesian coordinates the following identity is of use:

$$\nabla^2 A = \nabla^2 A = (\nabla^2 A_x)\bar{x} + (\nabla^2 A_y)\bar{y} + (\nabla^2 A_z)\bar{z} \quad \text{(EQ 3.3-6)}$$

We confine ourselves to the consideration of the homogenous vector wave equation, with no sources present, i.e.,

$$(\nabla_t^2 + n^2k^2 - \beta^2)e = -(\nabla_t + j\beta\bar{z})e_t \bullet \nabla_t ln(n^2) \quad \text{(EQ 3.3-7)}$$

and

$$(\nabla_t^2 + n^2k^2 - \beta^2)h = \{(\nabla_t + j\beta\bar{z}) \times h\} \times \nabla_t ln(n^2)\,. \quad \text{(EQ 3.3-8)}$$

where all the parameters of interest have been defined before. Now, on the basis of the vector identities (3.3-3) to (3.3-6), we see that the above equations (3.3-7) and (3.3-8) couple the field components for any coordinate system. Simplifications can be made to the above system if the Cartesian coordinate system is used as a reference, as well as using the principle of translational invariance. These results are presented as

$$(\nabla_t^2 + n^2k^2 - \beta_1^2)e_1 = -(\nabla_t + j\beta_1\bar{z}) \times (e_{tl} \bullet \nabla_t ln(n^2)) \quad \text{(EQ 3.3-9)}$$

and

$$(\nabla_t^2 + n^2k^2 - \beta_1^2)h_1 = -(\nabla_t ln(n^2)) \times (\nabla_t + j\beta_1\bar{z}) \times h_1\,, \quad \text{(EQ 3.3-10)}$$

where n is assumed to vary as a function of x and y only. Note that the scalar operator ∇ is used as opposed to the vector operator $\overline{\nabla}$ in equations (3.3-7) and (3.3-8). Also a point of confusion may be the use of the Cartesian unit vectors $\hat{x}$, $\hat{y}$ and $\hat{z}$. The spatial variation of

each of these components is directly translatable to a cylindrical coordinate system without loss of generality. The longitudinal field components e_{zl} and h_{zl} are also expressible by means of the coupled equations:

$$(\nabla_t^2 + n^2k^2 - \beta_1^2)e_{zl} - \frac{\beta}{(n^2k^2 - \beta_1^2)}(\nabla_t e_{zl} \bullet \nabla_t ln(n^2)) \qquad \text{(EQ 3.3-11)}$$
$$= -\sqrt{\frac{\mu_0}{\varepsilon_0}} \cdot \frac{k\beta_1}{(n^2k^2 - \beta_1^2)} \bar{z} \bullet (\nabla_t h_{zl} \times \nabla_t ln(n^2))$$

and

$$(\nabla_t^2 + n^2k^2 - \beta_1^2)h_{zl} - \frac{n^2k^2}{(n^2k^2 - \beta_1^2)}(\nabla_t h_{zl} \bullet \nabla_t ln(n^2)) \qquad \text{(EQ 3.3-12)}$$
$$= -\sqrt{\frac{\mu_0}{\varepsilon_0}} \cdot \frac{kn^2\beta_1}{(n^2k^2 - \beta_1^2)} \bar{z} \bullet (\nabla_t e_{zl} \times \nabla_t ln(n^2)),$$

where the index is translationally invariant. Examination of equations (3.3-9) to (3.3-12) reveals the reason for the various polarization phenomena, and the complexity of their description for weakly guiding waveguides. Under the weak guidance approximation, the value of the core index of refraction n_{co} and the cladding refractive index n_{cl} are approximately equal. A more rigorous proof of this is demonstrated in [Saf93] where the field solutions are used to calculate the amplitude ratios of the longitudinal (axial) field components to the transverse field components. This is shown to be of order $\Delta^{1/2}$ where

$$\Delta = \frac{n_{co}^2 - n_{cl}^2}{2n_{co}^2}. \qquad \text{(EQ 3.3-13)}$$

Since $\Delta << 1$, we see that the wave exhibits TEM-like behavior (no e_z or h_z) or approximately plane wave like behavior, i.e. the medium behaves like it is infinite and homogenous. However for a translationally invariant waveguide with a step profile, the RHS of equations (3.3-11) and (3.3-12) vanish in the core and the cladding, but not on the boundary. The general solution of the wave equation in such a case is the solution of the familiar Bessel's differential equation, in terms of Bessel functions.

In conclusion, the use of the Scalar Wave Equation (SWE) under the weak guidance approximation to solve for the value of the propagation constant gives only an approximate value, sufficient for all practical purposes. However, the issue of polarization

is not adequately explained. It is not the intention of this thesis to explore the ramifications of polarization, but to provide a justification for many of the assumptions that make the analysis more tractable.

3.3.2 The Scalar Wave Equation and the Gaussian Approximation

The calculus of variations is used in the solution of eigenvalue problems as detailed in [Sny81, Gre87, Mat70]. The mathematical formalism is non-trivial, and it suffices to say at this juncture that the intuitive variation of the fundamental mode field distribution is used as a trial function to calculate the largest eigenvalue β achievable. The largest value of β is that for the fundamental mode, and hence the trial function is an accurate representation of the field solution for the fundamental mode. In the selection of the Gaussian approximation for the analysis of the coupler problem, the selection was made on the basis of the fact that the formalism allowed use of both arbitrary profiles as well as provided closed form solutions for a Gaussian distributed index profile. Recall from the arguments in Chapter 2 that the variation of the index profile under conditions of isotropic thermal diffusion is Gaussian-like. This is particularly true for the case when an infinite medium is considered with a line source [Shi90]. Furthermore, as [Sny81] states, numerical solution of the SWE for the fundamental mode distribution reveals Gaussian-like behavior, i.e. with a maximum at the axis of the waveguide (remember that the cross-section of the guide is under consideration) and a smoothly decreasing amplitude as the radius increases. [Sny81] also goes on to state that the Gaussian approximation is useful for the analysis of fibers that have core and cladding materials diffusing into one another during manufacture. The analysis of the coupler based on the theory developed above as demonstrated by [Sny83] is presented.

The scalar wave equation for the radial dependence of the electric field reduces to the form

$$\left\{\frac{d^2}{dr^2} + \frac{1}{r}\frac{d}{dr} + k^2 n^2(r) - \beta^2\right\}\Psi = 0, \qquad \text{(EQ 3.3-14)}$$

under the weak guidance approximation. The trial solution for the application of the variational principle is:

$$\Psi_0(r) = exp\left(-\frac{r^2}{2r_0^2}\right). \quad \text{(EQ 3.3-15)}$$

where r_0 is the spot size, where the intensity should be *1/e* of the maximum. Substituting equation (3.3-15) into equation (3.3-14) and using the identity

$$rF_0\frac{d^2F_0}{dr^2} + F_0\frac{dF_0}{dr} = \frac{d}{dr}\left\{rF_0\frac{dF_0}{dr}\right\} - r\left\{\frac{dF_0}{dr}\right\}^2, \quad \text{(EQ 3.3-16)}$$

we see that the resulting stationary expression is

$$\beta^2 = \frac{\int_0^\infty \left\{-\left(\frac{d\Psi}{dr}\right)^2 + k^2n^2(r)\Psi^2\right\} r\,dr}{\int_0^\infty r\Psi^2 dr}. \quad \text{(EQ 3.3-17)}$$

To remove the dimensional dependence the dimensional parameters *U* and *V* are used, following standard convention in waveguide theory, where

$$U = \rho\sqrt{k^2n_{co}^2 - \beta^2} \quad \text{(EQ 3.3-18)}$$

and

$$V^2 = U^2 + W^2 = \frac{2\pi\rho\Delta}{\lambda}, \quad \text{(EQ 3.3-19)}$$

where

$$W = \rho\sqrt{\beta^2 - k^2n_{cl}^2}. \quad \text{(EQ 3.3-20)}$$

The factor ρ here is used as a scaling parameter. A word of explanation is needed about the scaling parameter. We may define a normalized radius R_0 defined as

$$R_0 = \frac{r_0}{\rho}. \quad \text{(EQ 3.3-21)}$$

For a continuous index profile the difficulty is in distinguishing between the core and the cladding, i.e. there is no well defined interface. Therefore the scaling parameter is adjusted for the Gaussian best fit approximation. The Gaussian profile is unique in the sense that the factor plays the same role as the spot size r_0 in the field distribution for the trial function. The spotsize is obtained by solving the following equation

$$\frac{\partial \beta^2}{\partial r_0} = 0. \qquad \text{(EQ 3.3-22)}$$

The trial function given by equation (3.3-15) is substituted into equation (3.3-17) to yield β_2 and this solution is used in (3.3-22). The value of r_0 is thus obtained. Once r_0 and β are known then the values of interest may be calculated from the equations:

$$E_x = exp\left(-\frac{r^2}{2r_0^2}\right)exp(-j\beta z) \qquad \text{(EQ 3.3-23)}$$

and

$$H_y = \sqrt{\frac{\varepsilon_0}{\mu_0}} n_{co} E_x. \qquad \text{(EQ 3.3-24)}$$

These equations are applicable to the *x*-polarized modes and the *y*-polarized modes are obtained by the application of duality. Again, it must be emphasized that since the scalar wave equation is under consideration, the polarization properties are not strictly reflected. The general equation for the index variation for a given profile function is

$$n^2(R) = n_{co}^2\{1 - 2\Delta f(R)\}. \qquad \text{(EQ 3.3-25)}$$

The normalization that is effected on the waveguide dimensions involves the scaling parameter

$$R = \frac{r}{\rho}. \qquad \text{(EQ 3.3-26)}$$

The equations for the modal parameters are then given by

$$U^2 = \frac{1}{R_0^2} + V^2\left\{ f(0) + \int_0^\infty \frac{df(R)}{dR} exp\left(-\frac{R^2}{R_0^2}\right) dR \right\} \quad \text{(EQ 3.3-27)}$$

and

$$\frac{1}{V^2} = \int_0^\infty \frac{df(R)}{dR} R^2 exp\left(-\frac{R^2}{R_0^2}\right) dR \quad . \quad \text{(EQ 3.3-28)}$$

For an arbitrary profile the field intensity *S* can be represented as

$$S = \frac{|a|^2}{2}\sqrt{\frac{\varepsilon_0}{\mu_0}} n_{co} exp\left(-\frac{R^2}{R_0^2}\right) \quad \text{(EQ 3.3-29)}$$

and the normalization *N* as

$$N = \frac{\pi\rho^2 n_{co}}{2}\sqrt{\frac{\varepsilon_0}{\mu_0}} R_0^2 . \quad \text{(EQ 3.3-30)}$$

The cutoff frequency is given by

$$V_c = 2.405\sqrt{2\int_0^\infty (1-f) R dR} . \quad \text{(EQ 3.3-31)}$$

For the special case of a Gaussian index profile, the equation for the spotsize r_0 is given by substituting the equation for the index variation given by equation (3.3-25) into equation (3.3-28) and solving to obtain

$$r_0 = \frac{\rho}{\sqrt{V-1}} . \quad \text{(EQ 3.3-32)}$$

3.3.3 Coupled Mode Analysis of Two Parallel Gaussian Index Profile Fibers

For a composite solution of two fibers placed near one another, the profile is given by

$$n^2 = n_{co}^2\left\{1 - 2\Delta\left[1 - exp\left(-\frac{r_1^2}{\rho_1^2}\right) - exp\left(-\frac{r_2^2}{\rho_2^2}\right)\right]\right\} \qquad \text{(EQ 3.3-33)}$$

where ρ_1 and ρ_2 are the scaling lengths and the profile n_{12} is given by equation (3.3-33) with the exponential in r_2 left out. We then apply equation (3.2-11) to find the coupling coefficient *C*. The dominant term in equation (3.2-11) comes from a region close to the axis of the second fiber, i.e. Ψ_2 is exponentially small over the core of the unperturbed fiber. To account for this from equation (3.2-9) we see that the general form of the coupling coefficient is

$$C = \frac{k\int_{A_\infty}(n - \bar{n}_1)\Psi_1\Psi_\pm \, dA}{\int_{A_\infty}\Psi_1\Psi_\pm \, dA}, \qquad \text{(EQ 3.3-34)}$$

where

$$\Psi_\pm = \Psi_1 \pm \Psi_2. \qquad \text{(EQ 3.3-35)}$$

To reiterate, the following assumption is made: n-n_1 vanishes over the core of the unperturbed fiber (fiber 1), i.e. from equation (3.2-10) and therefore $\Psi_1\Psi_2$ is the dominant term in the numerator. We then substitute for the index terms in equation (3.2-11) to get

$$C = \frac{k}{4N_1}\sqrt{\frac{\varepsilon_0}{\mu_0}}\int_0^\infty\int_0^{2\pi}\Psi_1\Psi_2 exp\left(-\frac{r_2^2}{\rho_2^2}\right)\cdot r_2 dr_2 d\phi, \qquad \text{(EQ 3.3-36)}$$

as justified above. Next we take advantage of the following identity,

$$k = \frac{V}{\rho n_{co}\sqrt{2\Delta}}. \qquad \text{(EQ 3.3-37)}$$

Using

$$R_2 = \frac{r_2}{\rho}, \qquad \text{(EQ 3.3-38)}$$

where the value of the scaling parameter is assumed to be equal for both fibers using symmetry arguments, we see that

$$C = \frac{Vn_{co}\rho}{4N_1} \cdot \sqrt{\frac{2\Delta\varepsilon_0}{\mu_0}} \int_0^{\infty} \int_0^{2\pi} \Psi_1 \Psi_2 exp(-R_2^2) \cdot R_2 dR_2 d\phi . \qquad \text{(EQ 3.3-39)}$$

Now make the substitution for the field distribution of the second fiber using equation (3.3-15) where the spotsize is obtained from equation (3.3-32) as

$$\Psi_2 = exp\left(-\frac{(V-1)}{2}R^2\right). \qquad \text{(EQ 3.3-40)}$$

Note that this is the near field distribution. An important issue may be raised at this juncture. Ψ_1 corresponds to the perturbing fiber and Ψ_2 corresponds to the perturbed fiber. The value of the cladding index decreases exponentially with respect to the core index as we move away from the axis of the waveguide. This is confirmed on the basis of the solution of the diffusion equation. Thus, away from the axis of the perturbing fiber we have to consider the far or evanescent field of Ψ_1 especially in the analysis of an optical fiber coupler where good optical separation has been assumed as a necessary condition for the analysis. Thus it is expressed in more quantifiable terms. The scalar wave equation when solved for the uniform cladding assumption yields the solution in terms of the modified Bessel function $K_0(WR)$ where all the parameters of interest have been defined before. Using the large argument approximation of this function we can see the explicit exponential behavior when $WR>>1$:

$$K_\upsilon(z) \cong \sqrt{\frac{\pi}{2z}} exp(-z)\left\{1 + \frac{4\upsilon^2 - 1}{8z}\right\}. \qquad \text{(EQ 3.3-41)}$$

Thus a modification to the Gaussian approximation must be made to calculate the far field pattern. This may be done by substituting the profile function into the scalar wave equation which is rewritten in terms of the modal parameter W defined earlier in equation (3.3-20) as well as the index profile representation for an arbitrary fiber $f(R)$ as

$$\left\{\frac{d^2}{dR^2} + \frac{1}{R}\frac{d}{dR} - W^2\right\}\Psi = -V^2(1-f)\Psi . \qquad \text{(EQ 3.3-42)}$$

The value of *f* exhibits a maximum value of 1 in the cladding. Thus the correction here is applicable to the region near the fiber axis where the Gaussian approximation holds, (i.e. the RHS is significant) and we thus may replace the expression for Ψ on the RHS with the explicit exponential dependence predicted by the trial function given by equation (3.3-15). Equation (3.3-42) may be rewritten as:

$$\left\{\frac{d^2}{dR^2}+\frac{1}{R}\frac{d}{dR}-W^2\right\}\Psi = -V^2(1-f)exp\left(-\frac{R^2}{2R_0^2}\right). \qquad \text{(EQ 3.3-43)}$$

Using Green's function Methods the following results are presented. The solution of the equation having the form

$$\nabla_t^2\Psi + (k^2n^2-\beta^2)\Psi = \chi, \qquad \text{(EQ 3.3-44)}$$

where χ is a function of the radial position across the fiber is discerned by use of the Green's function *G(r,r')* of this equation. After suitable boundary conditions are applied, the Green's function satisfies

$$(\nabla_t^2 + k^2n^2-\beta^2)G = \delta(r-r'), \qquad \text{(EQ 3.3-45)}$$

given that the position *r'* is fixed and δ denotes the Dirac delta function. The solution of equation (3.3-44) reduces to the integral over the volume for non-zero χ as:

$$\Psi(r) = \int_V G(r,r')\chi(r')dV'. \qquad \text{(EQ 3.3-46)}$$

For the case of the far field pattern using the scalar wave equation for the Gaussian approximation equation (3.3-44) assumes the form

$$\left\{\frac{d^2}{dR^2}+\frac{1}{R}\frac{d}{dR}-W^2\right\}G = -\delta(r-r'), \qquad \text{(EQ 3.3-47)}$$

where the Green's function *G(R,R')* is given by

$$G(R,R') = -K_0(WR)I_0(WR')R', \qquad 0 \le R' \le R \qquad \text{(EQ 3.3-48)}$$

$$= -I_0(WR)K_0(WR')R', \qquad R \le R' \le \infty.$$

From equation (3.3-46) we see that the solution is

$$\Psi(r) = -K_0(WR)\int_0^R I_0(WR')\chi(R')R'dR' \qquad \text{(EQ 3.3-49)}$$
$$-I_0(WR)\int_R^\infty K_0(WR')\chi(R')R'dR'.$$

χ(R') is of the form of the RHS of equation (3.3-43). The key point to note here is that the second integral's contribution away from the fiber axis is negligible due to earlier arguments and hence may be neglected. The far field pattern for Ψ_1 is then given by

$$\Psi(R) \cong V^2 K_0(WR)\int_0^R R'\{1 - f(R')\}I_0(WR')exp\left(-\frac{R'^2}{2R_0^2}\right)dR'. \qquad \text{(EQ 3.3-50)}$$

For the Gaussian profile where the index variation is given by substituting into equation (3.3-25) as

$$f(R) = 1 - exp(-R^2), \qquad \text{(EQ 3.3-51)}$$

we get

$$\Psi_1(R) = \frac{V^2}{V^2+1}K_0((V-1)R)exp\left\{\frac{(V-1)^2}{2(V+1)}\right\}. \qquad \text{(EQ 3.3-52)}$$

The expressions for Ψ_1 and Ψ_2 are substituted into equation (3.3-39) as

$$C = \frac{\sqrt{2\Delta}}{\rho}\cdot\frac{V^3(V-1)}{(V+1)}exp\left\{\frac{(V-1)^2}{2(V+1)}\right\}\cdot \qquad \text{(EQ 3.3-53)}$$
$$\int_0^{2\pi}\int_0^\infty K_0((V-1)R_1)exp\left\{-\frac{(V-1)^2}{2}R_2^2\right\}R_2 dR_2 d\phi_2.$$

Now the formula

$$K_0(ar_1)\cos(m\phi_1) = \sum_{p=-\infty}^{\infty} \text{sgn}(p)K_{p+m}(ad)I_p(ar_2)\cos(p\phi_2) \qquad \text{(EQ 3.3-54)}$$

is applied. This nomenclature applies to that described by Fig. (3.2-1). Note that we take *m* to be zero and that once the integration is performed over ϕ_2, the resulting terms of the form *sin(p)/p* vanish except when *p* is zero. Therefore equation (3.3-53) reduces to

$$C = \frac{\sqrt{2\Delta}}{\rho} \cdot \frac{V^3(V-1)}{(V+1)} exp\left\{\frac{(V-1)^2}{2(V+1)}\right\} \cdot K_0\left\{\frac{(V-1)d}{\rho}\right\} \int_0^\infty I_0\{(V-1)R_2\} exp\left\{-\frac{(V-1)^2}{2}R_2^2\right\} R_2 dR_2 . \quad \text{(EQ 3.3-55)}$$

Now the formula

$$\int_0^\infty z I_0(bz) exp(-a^2 z^2) dz = \frac{exp(b^2/4a)}{2a^2} \quad \text{(EQ 3.3-56)}$$

may be used to evaluate the integral so that equation (3.3-55) reduces to

$$C = \frac{\sqrt{2\Delta}}{\rho} \cdot \frac{V^3(V-1)}{(V+1)^2} exp\left\{\frac{(V-1)^2}{(V+1)}\right\} \cdot K_0\left\{\frac{(V-1)d}{\rho}\right\} \cdot \quad . \quad \text{(EQ 3.3-57)}$$

4 Evaluation of the Model

4.1 Comparison of the Gaussian Approximation with the Step Index Approximation

The motivation to look at two different ways of modeling the coupling behavior arises from the fact that two types of coupling behavior are generally exhibited. For Fused Biconical Tapered (FBT) couplers, the predominant method of manufacture, it is not uncommon to have the coupler go through multiple power exchange cycles [McL88] in the course of its fabrication. The predominant coupling mechanism there is the reduction in core size, as evidenced by the elongation of the interaction region. The tapered region can grow by up to 200% in some cases. The action has been successfully modeled [Bur88] as the field spreading due to a decrease in the value of V driven by the core size reduction. The index values are assumed to remain constant.

This analysis is no doubt appropriate for the *strong coupling* regime, where multiple power exchange cycles are exhibited. However, the intention of this evaluation was to examine the *weak coupling* regime, as an alternative means of coupler manufacture. This would imply on the order of one crossover. Practically, to enforce this, the assumption that the core sizes do not change had to be ensured. To do this, a specially designed platinum wire *Pac-Man* furnace (see Fig. 4.2-2) was used to diffuse the fibers. The increase in taper length was restricted to 20%.

Other authors [McL88] have investigated the phenomenon of diffusion for the tapered coupler in the weakly coupled regime with some success. However, to the best of the author's knowledge, the question of fabrication of a non-tapered coupler (practically, this is difficult to enforce; an increase in length about 20 percent is anticipated due to the axial stress that needs to be maintained to ensure that the minimum taper region does not buckle while being heated) has not been investigated. One way to analyze this would be to extend the model due to [McL88] for the non-tapered coupler. This is attempted in the following section on the *step index approximation*. Initial investigations raised questions on the applicability of this model, and it was decided that the *gaussian approximation* would be a more suitable candidate for this analysis. This is due to the fact that the gaussian approximation enables the use of a scaling parameter ρ on the radius of the fiber. This is important as it couples the decrease in index (and consequent change in the *step*

index delta) to the varying effective radius. No clear cut core-cladding interface exists, and minimum and maximum values may be used in conjunction with the scaling parameter ρ. This approximation is verified by evaluating the spot-size r_0 in the Gaussian approximation and using this as an indicator of ρ as demonstrated in section (4.1.3) below.

4.1.1 The Step Index Approximation

Since diffusion is a mass transport phenomenon, we know that the mass of the diffusing substance remains constant. Consider a cylindrical structure as shown in Fig (4.1-1).

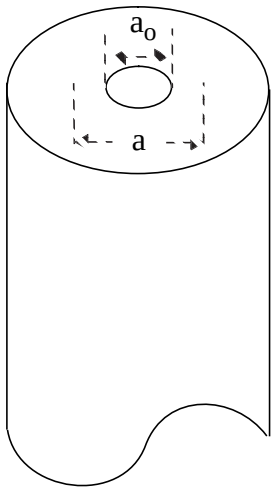

FIGURE 4.1-1 Cross-section of an optical fiber showing the radius post and pre-diffusion

The volume of the inner region over a height *z*, defined as our coupling interaction length, is given by

$$M = \pi a_0^2 z \qquad \text{(EQ 4.1-1)}$$

where *M* denotes the volume and a_0 is the radius of the core. Given that the mass remains constant, we see that there is a change in the density corresponding to the increased volume after diffusion. Using the expressions for density, and equating the masses we see that

before diffusion and after diffusion, we may write

$$\pi a^2 z d = \pi a_0^2 z d_0 \qquad \text{(EQ 4.1-2)}$$

or

$$a = a_0 \sqrt{\frac{d_0}{d}} \qquad \text{(EQ 4.1-3)}$$

where d_0 and d are the densities before and after diffusion and a is the new core radius. Now we may get an indication of the various densities from the numerical simulation of the diffusion equations shown for various times in Fig. (4.1-3) for a *Ge* doped matched clad fiber, based on equation (2-3-4). The first 95 terms of the roots of the Bessel function are taken to ensure stability of the solution. The peak concentration, which is proportional to the dopant concentration, is an indication of the density. Strictly speaking, this is true only for a step index profile, but can be applied to the Gaussian profile since solutions are insensitive, under the equal profile volume concept [Sny83], to profile volume changes to the first order. We then calculate the new values of the core radii and use these in the calculation of the various coupling coefficients

4.1.2 Formulation of the Step Index Crosstalk Expression.

These results are shown without proof and can be found in any standard textbook on optical waveguide theory [Ada81]. [Sny83] presents the coupling coefficient defined in a manner similar to that in Chapter 3 as

$$C = \frac{\sqrt{2\Delta}}{a} \cdot \frac{U^2 K_0(Wd/a)}{V^3 K_1^2(W)} \qquad \text{(EQ 4.1-4)}$$

for crosstalk between two identical (or very nearly so) fibers, where all the parameters of interest have been defined before. *d* in this case is the separation between the fibers as shown in Fig. (4.1-2).

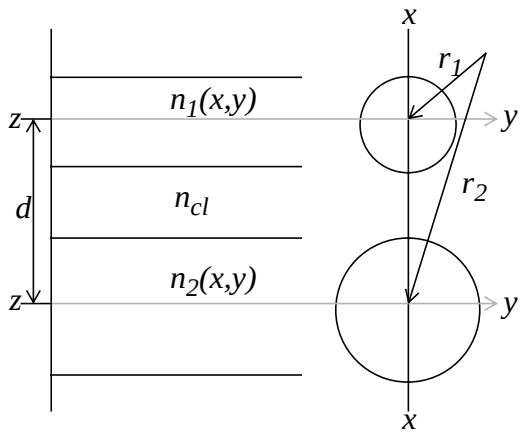

FIGURE 4.1-2 Coordinate System for Crosstalk Analysis

Note that the solution for the value of U requires that the eigenvalue equation given by

$$\frac{J_0(U)}{UJ_1(U)} = \frac{K_0(W)}{WK_1(W)} \qquad \text{(EQ 4.1-5)}$$

where

$$U = k_0 a \sqrt{n_{co}^2 - \beta^2} \qquad \text{(EQ 4.1-6)}$$

and

$$W = k_0 a \sqrt{\beta^2 - n_{cl}^2} \qquad \text{(EQ 4.1-7)}$$

is satisfied.

We solve for $k_0 a$ from the expression

$$k_0 a = \frac{V}{\sqrt{n_{co}^2 - n_{cl}^2}}. \qquad \text{(EQ 4.1-8)}$$

The eigenvalue equation is solved numerically for the propagation constant. A combination of the bisection method and a variation of Newton's Method was used. Thus, for V=1.5, Fig. (4.1-7) plots the variation of the dimensionless parameter $Ca/\sqrt{2\Delta}$ against *d/a* where *d* is the separation between the fibers and *a* is the core radius. As the diffusion proceeds, the core radius increases.

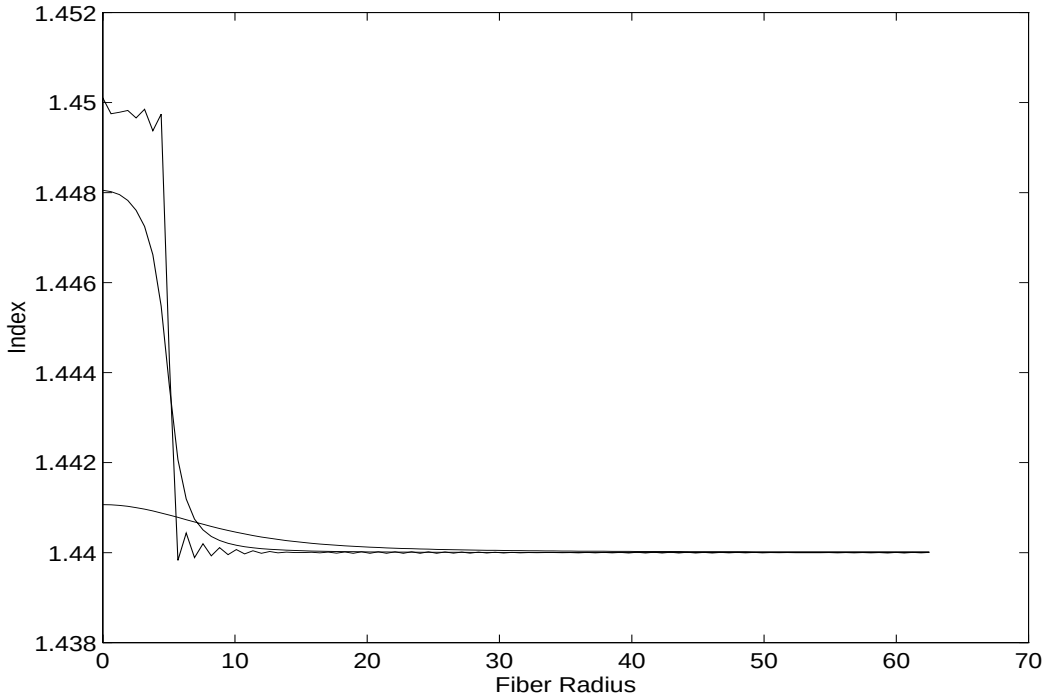

FIGURE 4.1-3 Variation in the Index Profile for Heating Times of 100s, 1000s and 10000s.

The values of the index as a function of heating time are shown in Fig. (4.1-3) based on parameter values set as detailed in the section below.

4.1.3 The Gaussian Approximation

For evaluation of the gaussian approximation, the field solution is given by equation (3.3-23). In order to compare the step index approximation with the gaussian approximation, the similarity between the spotsize r_0 and the scaling parameter ρ is exploited. We equate the radial function *f(R)* to the concentration distribution *C* predicted by equation (2.3-4) where,

$$f(R) = 1 - \frac{C}{C_0} \qquad \text{(EQ 4.1-9)}$$

for germania doped fibers and

$$R = \frac{r}{\rho}. \qquad \text{(EQ 4.1-10)}$$

Thus the coupling coefficient is given by

$$C = \frac{\sqrt{2\Delta}}{\rho} \cdot \frac{V^3(V-1)}{(V+1)^2} exp\left\{\frac{(V-1)^2}{(V+1)}\right\} \cdot K_0\left\{\frac{(V-1)d}{\rho}\right\} \quad . \qquad \text{(EQ 4.1-11)}$$

We know from equations (4.1-10) and (2.3-4) that

$$f(R) = \frac{a^2}{b^2} + \frac{2a}{b^2}\sum_{n=1}^{\infty} exp(-D\alpha_n^2 t) \times \frac{J_0(R\alpha_n)}{\alpha_n J_0^2(b\alpha_n)} \cdot J_1(a\alpha_n) \quad . \qquad \text{(EQ 4.1-12)}$$

From equation (3.3-25),

$$n^2(R) = n_{cl}^2 \cdot f(R) + n_{co}^2(1 - f(R)) \quad . \qquad \text{(EQ 4.1-13)}$$

We solve for the value of the spotsize from equation (3.3-28) and the formula

$$\int_0^{\infty} exp(-a^2t^2)t^{\nu+1}J_\nu(bt)dt = \frac{b^\nu}{(2a^2)^{\nu+1}} exp(-b^2/4a^2) \quad , \qquad \text{(EQ 4.1-14)}$$

to get

$$\frac{1}{V^2} = \frac{R_0^4}{2b^2}\sum_{n=0}^{\infty} \alpha_n^2 \frac{J_1(a\alpha_n)}{J_0^2(b\alpha_n)} exp(-D\alpha_n^2 t) exp\left(-\frac{\alpha_n^2 R_0^4}{4}\right) \quad . \qquad \text{(EQ 4.1-15)}$$

When equation (3.3-28) is applied, note that the order of integration and summation is changed. This is valid as the infinite series representation of *f(R)* given by equation (4.1-2) is convergent. We see this by the application of the *Weierstrass M-test*. It is well known that the exponential function of a real variable has a greater rate of convergence than any power of that variable. When we consider the function represented by the terms involving the Bessel functions, it is possible to bound these by the moduli of $J_0(x)$ and $J_1(x)$ and observe that the series are convergent. Alternatively, the series expansion of $J_v(x)$ [Abr70] could be used to apply the ratio test, to prove the same result. The mathematical details are neglected for brevity. A simple application of the ratio test to study the absolute convergence of the series was attempted, and proved. A satisfactory evaluation of the summation was found to work over the first 95 terms of the zeros of the function:

$$J_1(b\alpha_n)\ . \qquad \text{(EQ 4.1-16)}$$

One important factor was the error analysis in the function evaluation. Numerical results for the error analysis of equation (4.1-16) are shown in Fig. (4.1-4).

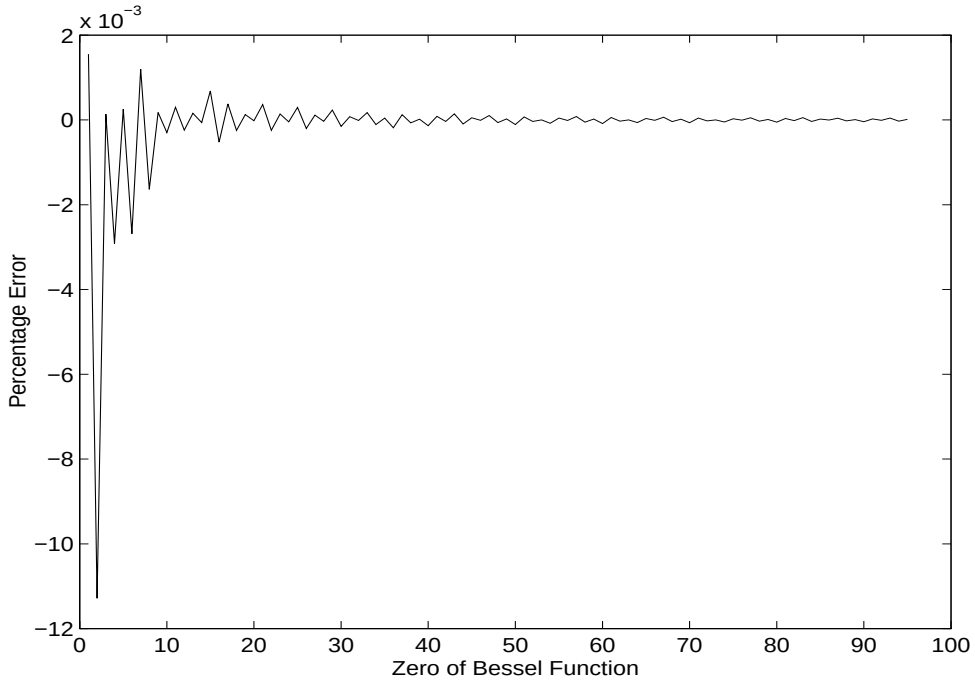

FIGURE 4.1-4 Percentage Error in the Root Evaluation

Note that the error is greater for the initial zeros, but this was acceptable in that no significant changes in the analysis was evidenced by further improvements in the errors. We are interested in the behavior of a series having the general form of the *Dini Expansion:*

$$\sum_{n=1}^{\infty} b_n J_1(\lambda_n(a/b)) \qquad \text{(EQ 4.1-17)}$$

where

$$\lambda_n = b\alpha_n, \qquad \text{(EQ 4.1-18)}$$

and we are interested in the behavior of the series as $n \to \infty$. The series passed the ratio test for an acceptable value of ε and the trade-off between computer speed and error was made. The coefficient b_n is expressible in integral form, and the analytical evaluation is not carried out as numerical methods are more tractable.

The next step was to examine the time evolution of the index variation as predicted by equation (4.1-13) for the parameters described above. Diffusivity data in the literature is scarce and one reference [Kra86] was chosen for the value of *D*. Since the coupling interaction length is fixed, any power oscillations predicted by the theoretical results will have to include the time factor. The diffusion coefficient is temperature dependent and we follow the assumption due to [Bot88] that the variation is an Arrhenius relationship given by

$$\log(D) = \log(D_0) - \frac{K}{T}\ , \qquad \text{(EQ 4.1-19)}$$

where D is the diffusion coefficient, D_o and K constants found by experimental fits to measured data [Kra86] and measured data and T is the absolute temperature in degrees kelvin (K).

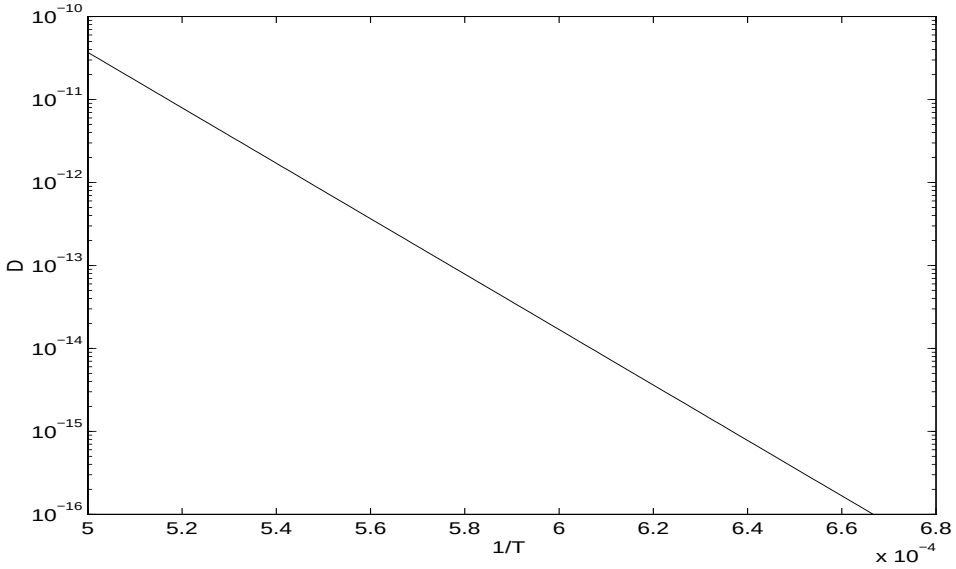

FIGURE 4.1-5 Variation of the Diffusion Coefficient for GeO_2 in SiO_2 with Temperature

This is indicated for germania in Fig. (4.1-5), where $g = 3.34102 \times 10^4$ and $log(D_0) = 6.273$. A value of $t = 100$ seconds and $D = 1 \times 10^{-15}$ m^2s^{-1} is used. Perturbation analysis revealed that the small variation in D does not impact the variation in the coupling coefficient, especially for larger values of time. Using these parameters, the index variation was computed for different values of time, spaced an order of magnitude apart, i.e. 100 s, 1000 s and 10000 s. This is indicated in Fig. (4.1-3). For the purposes of simulation, core and cladding indices of 1.45 and 1.44 were assumed as typical values. A pure Germania core was also assumed, as this is the most common fiber type used in coupler manufacture.

The next step was to solve equation (4.1-15) numerically to evaluate the normalized spotsize R_0. We defined the spotsize r_0 as given by the field solution in equation (3.3-15) where the normalized spotsize is given by equation (3.3-21). For a gaussian best fit, the value of the spotsize given by equation (4.1-15) is normalized and hence the radius of interest b, has to be normalized by the same parameter ρ using equation (4.1-10). The value of the parameter V is fixed. This is not unreasonable as can be

demonstrated from physical arguments. For fibers of small *V,* the spread of power is non-negligible away from the fiber axis. Simulations on the time of interest (i.e. the diffusion times) and the values of diffusion coefficient reveal a negligible variation in delta for the value *V,* defined as

$$V = \frac{2\pi a n_{co}\sqrt{2\Delta}}{\lambda}. \qquad \text{(EQ 4.1-20)}$$

Thus *V* remains substantially constant over the range of heating times and diffusion coefficients, even though the profile shape may change considerably, and it is safe to assume that the fundamental mode uniquely exists and therefore the theoretical developments in Chapter 3 are applicable. Under the Gaussian approximation, *V* has to be greater than 1, yet for single moded operation *V* should be less than 2.592 [Sny83]. This thesis concentrates on a value of *V*=1.5 though any appropriate number in the open interval (1, 2.592) could have been chosen. Using this value of *V* the RHS of (4.1-15) is evaluated and plotted in Fig. (4.1-6).

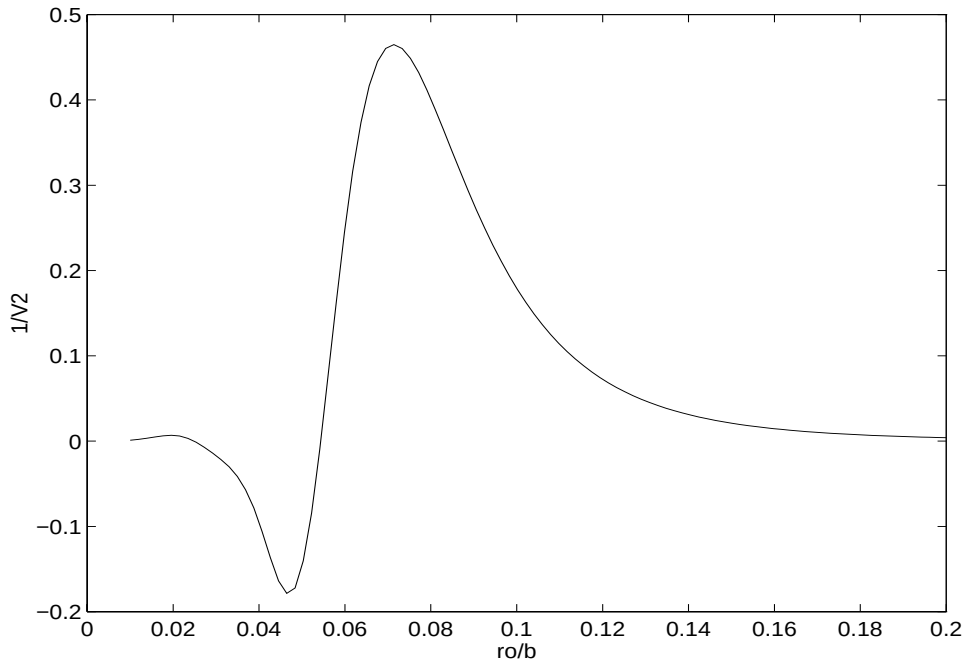

FIGURE 4.1-6 $1/V^2$ as a Function of the Spotsize (r_o/b)

This shows the solution for the limiting value of ρ that ensures a solution to the equation for *V*=1.5. This is of course a two valued function as expected (i.e. there are two roots, and hence two values for the normalized spotsize). The scaling parameter is the dependent variable on which basis the equation is solved. We may consider the solution for other values of *V,* on the basis of experimental evidence, for the weakly coupled case, but restrict consideration to *V*=1.5 in the absence of a near field scan of experimentally generated data from the cross-section of a fiber across its minimum taper region. The value of the scaling parameter thus obtained for the Gaussian best fit approximation was 4.2373.

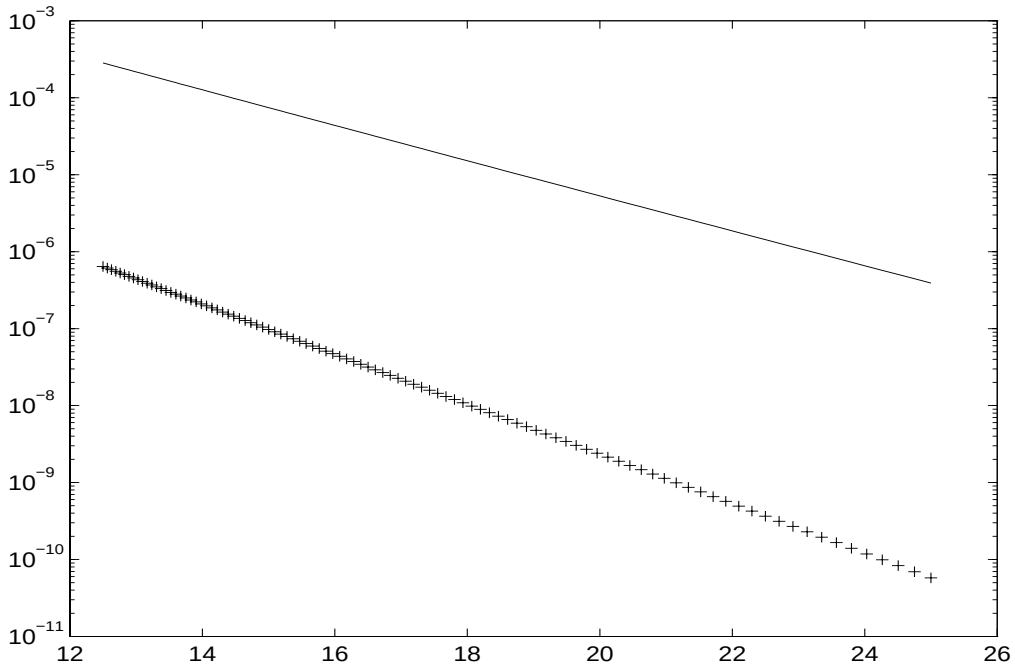

FIGURE 4.1-7 Coupling parameter variation with d/ρ for Gaussian Approximation (-) and Step Index Approximation (+)

Finally, within the gaussian approximation the coupling coefficient predicted was calculated using equation (4.1-11). This is plotted in Fig. (4.1-7) along with the results predicted by the equivalent step index approximation. As is shown there are about 2 to 3 orders of magnitude difference in the result.

4.2 Experimental Verification of the Model

The theoretical analysis of coupler manufacture is complicated for a variety of reasons. The proof of the pudding in terms of experimental verification of any proposed model is inherently hampered by the fact that a multiplicity of factors are involved. Isolating the effects of any one process requires that controlled environments are required which is difficult to enforce in practice. Based on experimental observations, three major problems are encountered in the manufacture of coupler using the dopant diffusion technique. First the problem of maintaining good contact between two fibers without overheating of the twists, if the fibers are twisted together before diffusion, has to be solved. This was done by twisting the fibers initially to fuse them together quickly using an oxy-propane torch. Then the twists are removed. This is a process that has to be done very carefully as the taper region is extremely fragile. The initial length is fixed at this stage.

The second problem requires that there be an approximately constant temperature spread across the coupling interaction length. This is achieved by heating the coupling interaction length in a specially designed diffusion furnace as shown in Fig. (4.2-1). This is constructed using a ceramic shell with a coil former to hold a platinum wire heating coil. Insulation is provided using glass wool packing. Ideally, all such experiments should have been done in an evacuated chamber. Also temperature measurement should be done using a pyrometer. The coupling interaction region should be coated with carbon to improve emissivity. However as this was a proof of concept experiment, it was decided that the fibers could be exposed to air.

Thirdly, a constant axial stress should be applied to the fibers during diffusion. The purpose of this is to accelerate the diffusion process [McL88] as well as to ensure that the fibers do not sag during the diffusion process. However the stress should not taper the interaction region. In practice this is difficult to enforce. As we were looking for an interaction length of 6 mm to ensure adiabaticity, the initial length was fixed at 5 mm, and the coupling interaction region was allowed to grow to 1 mm to compensate for sag.

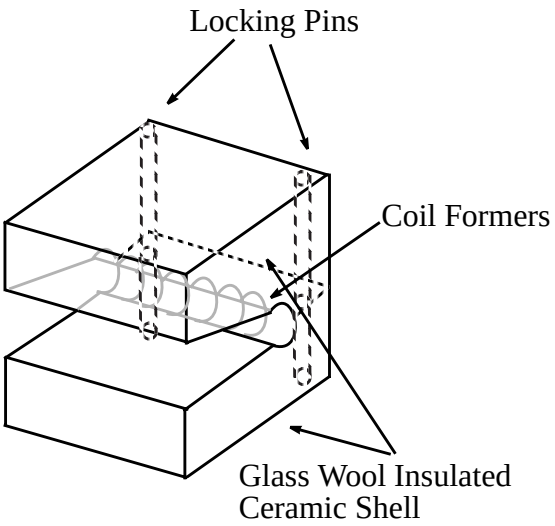

FIGURE 4.2-1 Block Schematic of Pac-Man Diffusion Furnace

This was done using a fiber tapering station shown in Fig. (4.2-2).

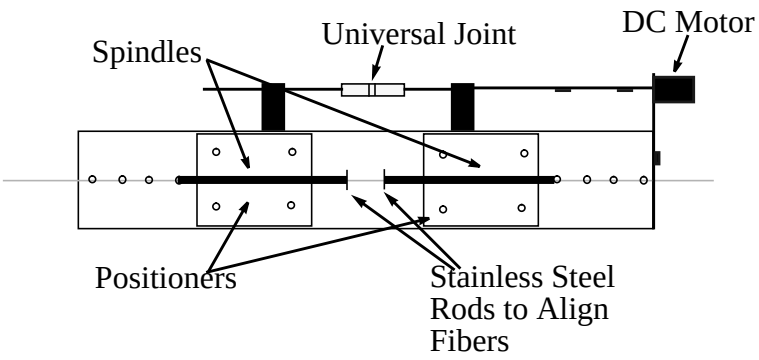

FIGURE 4.2-2 Coupler tapering Stage used to Support Fibers during Diffusion [Vup94]

This consists of two travelling position stages driven by a dc motor. The relative positions of the stages can be adjusted along a rail and a foot pedal controls the motor operation. A human operator controls the sag of the fibers during diffusion.

Experimental verification of the model was attempted using step index GeO_2 doped SMF at 1.3 μm. Fiber type SMF-028 manufactured by Corning Glass Works, Corning, New York was used. A block diagram of the system is indicated in Fig (4.2-3). Power was monitored on a 4 port UDT S390 optical power meter with data acquisition support provided by a GPIB/IEEE-488 bus to read power at 1 second intervals.

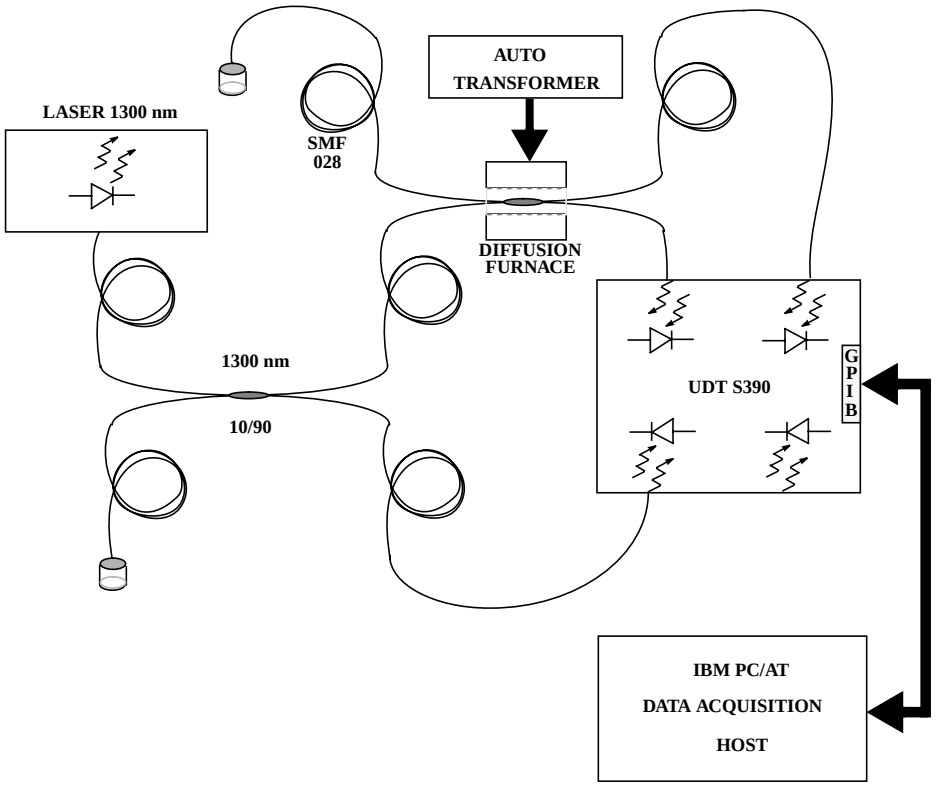

FIGURE 4.2-3 Block Diagram of the Experimental Setup

A number of single mode 2x2 couplers were made on a coupler station that allowed

tapering control. A 1.3 μm laser diode source was used, and the wavelength dependence of the source was measured using a white light source and an optical spectrum analyzer. The platinum wire diffusion furnace was used to diffuse the fibers. Based on the fiber survivability over extended periods of heating at high temperatures, as well as the index variation simulations (Fig. (4.1-3)) a maximum diffusion time of 1000 seconds was thought to be practicable. This has been borne out in actuality. The experimental details are shown photographically in Figs. (4.2-4) and (4.2-5).

FIGURE 4.2-4 View of the Diffusion Furnace and the Tapering Stage

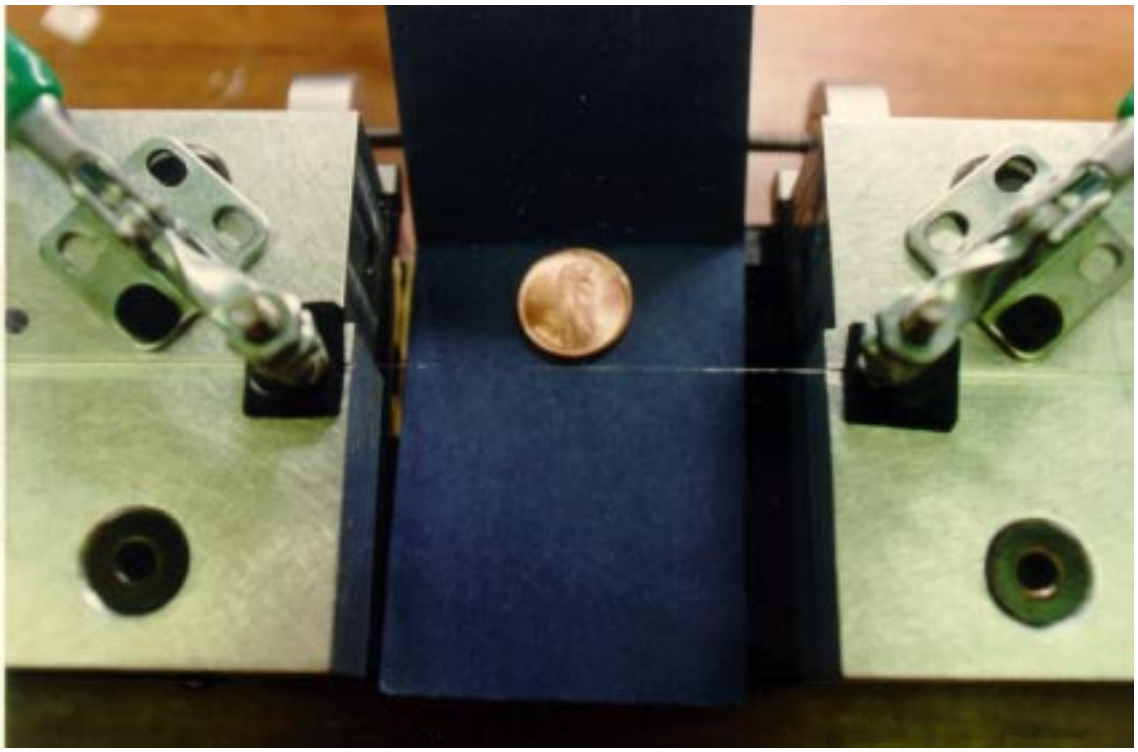

FIGURE 4.2-5 View of the Diffused Coupler mounted on the Tapering Stage

4.2.1 Procedure

Normally when Fused Biconical Tapered Couplers are manufactured, the fibers are twisted together prior to fusion. This ensures that the fibers remain in intimate contact as the fusion process proceeds. It is fairly well known [Gun94] that the primary coupling mechanism is due to the tapering action, and that the losses in the twists are negligible. However, if the twists are diffused, then the localized variation of the index at the twists causes the loss of the inherent parallel waveguide structure, due to dopant diffusion, and the twists exhibit considerable losses. Initially, the experiments were done using twists as it was hoped that the coupling due to dopant diffusion would manifest itself over a given time interval, before the excess losses rendered the coupler useless as the diffusion proceeded. The next series of experiments were done with the removal of the twists, after initial contact had been made due to the fusion of the fibers. This is fairly arduous to achieve in practice as the glass becomes extremely brittle at the twists. However, as expected, complete power transfer was achievable when this was done.

The initial length of the interaction was fixed at 5 mm and increased to 6 mm as the fibers were pulled. Tapering was stopped after 6 mm was reached. The throughput/non-throughput fiber split was approximately placed at 60%/40%. A figure of 6 mm was decided on to ensure that the tapering would be adiabatic, as according to [Lov87] a figure of 3 mm is needed for a single taper to be adiabatic for standard 1.3 μm telecommunications grade fiber. Furthermore, on diffusion, the adiabaticity condition would be further improved due to the increased core broadening. The interaction region was then heated in the platinum wire furnace at 1200°C. While care was taken to ensure that the finite ramp time of the heating was accounted for, including minimization of thermal shock effects on the furnace, it must be borne in mind that the temperature values are not precise. It is suggested that any future experiments that conducted be done with a pyrometer, and that the coupling region be placed in a vacuum and coated with carbon to improve the emissivity of the minimum taper region. An approximately three minute transportation lag was found to exist for a step change in voltage in the autotransformer control voltage.

4.2.2 Experimental Results

Two experiments that were considered representative of the results achieved are presented, and the time evolution of the coupled power is examined to elucidate the coupling behavior. The first type of experiment with the twists in place is indicated in Fig. (4.2-6) and is an example of the twisted diffused coupler detailed above. The results of the second type of experiment (i.e. without twists) are indicated in Fig (4.2-7).

Figs. (4.2-6) and (4.2-7) show the variation of coupled power in the various arms of two single mode couplers. Fig. (4.2-6) shows variation in the coupled power for a coupler made with twists according to the above procedure, at 1200° C. After about 375 seconds, it was seen that the effects of diffusion become pronounced. The coupler goes through two crossovers, and after about 600 seconds the excess loss starts dominating to the point where it was decided that continuation of the coupler manufacture would be of little use. This behavior is attributed due to the dopant diffusion at the point where the fiber is twisted [Gun94] and the coupler begins to become very lossy. Note that the coupler's crossovers do not exhibit total power transfer, signifying weak coupling. The process of the crossovers takes place in about 50 seconds, indicating a sinusoidal variation in power coupled with a period of about a 100 seconds. Insufficient data exists to draw further valid conclusions about the coupling mechanism, due to the inability of the experimentalist to obtain index profiles showing the concentration as a radial function of distance across the coupling region.

The next series of experiments were attempted with removal of the twist. Fig. (4.2-7) shows the variation in powers for the first 600 seconds. Note that the coupling mechanism seems much weaker than that for the previous case. This is felt to be due to the removal of any tension on the fiber due to the untwisting process. However, the excess loss remains fairly constant proving that the twist was responsible for the higher losses. As [McL88] theorizes, the slower diffusion may be due to the fact that stress accelerates diffusion. However, the process is not well understood and the behavior of vitreous materials at elevated temperatures is not the focus of this thesis. An interesting point to note, as illustrated in Fig. (4.2-7) is that almost total power transfer has taken place. Extreme bend sensitivity is noted at points approximately 75, 175 and 275 seconds on Fig.

(4.2-8) on the twisted coupler. This is due to the sagging of the fiber, and the interaction of the operator in order to ensure that sufficient axial tension was present. However, on the introduction of an external perturbation to the coupling region, in terms of an index differential, no change in the power is noted. This seems to signify that the core broadening has made the coupler extremely sensitive to bends, but the assumption of an infinite cladding is still valid.

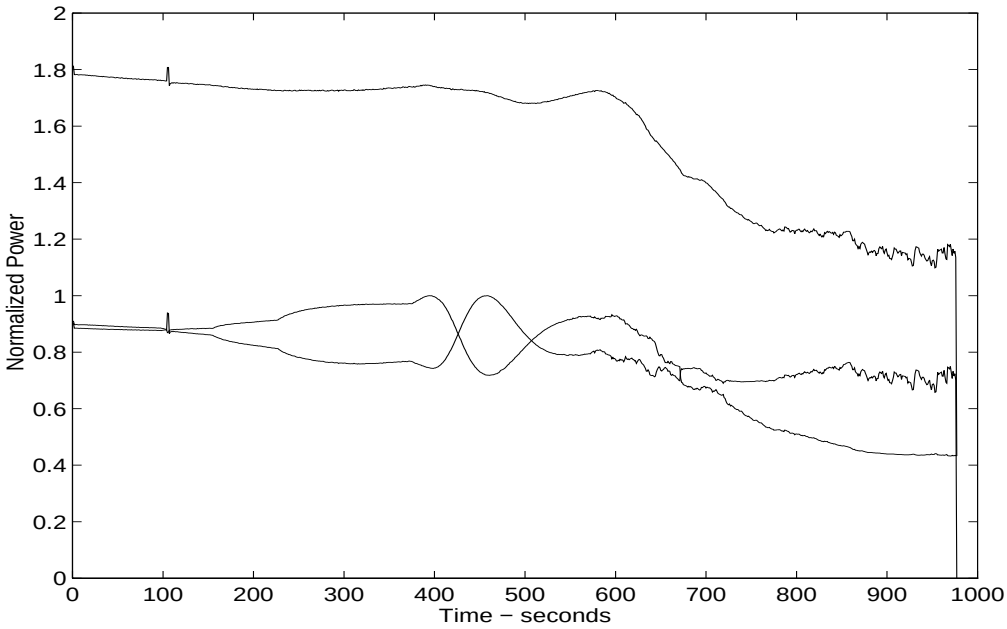

FIGURE 4.2-6 Measured Time Evolution of a 2x2 Single Mode Coupler; Top Trace is the Sum of the Branch Powers.

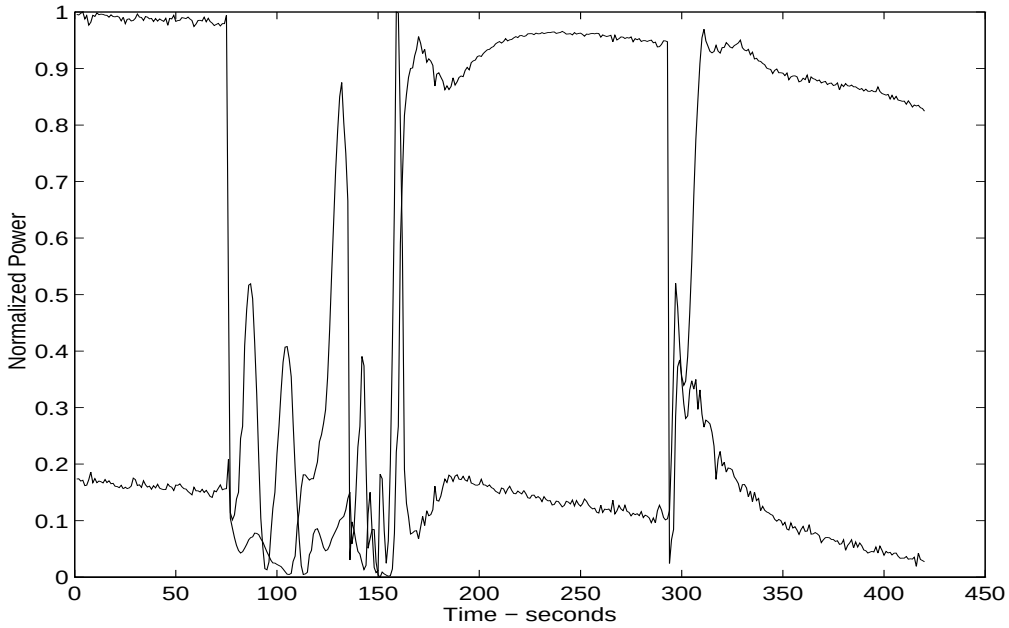

FIGURE 4.2-7 Time Evolution of a Coupler with Removal of the Twists

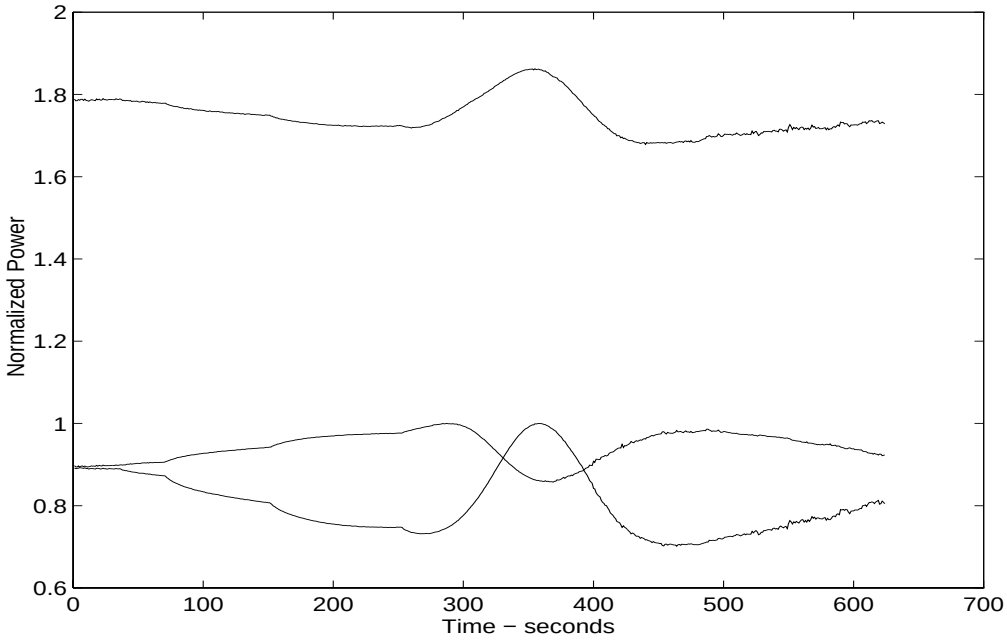

FIGURE 4.2-8 Bend Sensitivity of the Coupler in Figure (4.2-6)

4.3 Comparison of Experimental Results and Theoretical Results

As we are looking at the weak coupling regime, we are interested in the behavior the coupler exhibits over one crossover. It follows from this that if we define the beat length as the distance over which one complete power exchange cycle takes place, then by knowing the interaction length we can predict the coupling coefficient required for that beat length. It is important to note that we are predicting the time evolution of the coupler, and relating it to the spatial variation in the index distribution. This is valid only if the time constants are such that uniformity in C can be expected in relation to the overall time of diffusion. Thus the selection of the time of diffusion is paramount. Earlier studies have used different fiber types at different temperatures and different times of diffusion. [Kra86] diffused fiber sections for relatively shorter periods of time (tens of seconds and higher) at higher temperatures while [Bot88] did this at lower temperatures for longer periods of time (tens of minutes), albeit for a different dopant. We selected a value intermediate between the two. We were interested in the behavior of a coupler over a typical range of 100 seconds based on our numerical simulations. Examination of the data gathered above revealed that the Gaussian approximation could be used to generate a value of C consistent with that generated experimentally as shown in Fig (4.3-1).

As is seen, the behavior, while not perfect predicts the time evolution of the coupler fairly well from qualitative arguments. The initial change in behavior can be attributed to the sagging of the fiber and the intervention of the operator to correct this, as detailed in the section (4.2.2) above on bend sensitivity. The deviation in the latter stages is due to the breakdown of our inherent assumption that the time constant is favorable. This is akin to saying that the assumption that the d/ρ ratio in equation (4.1-11) is relatively constant breaks down. Further modeling of this phenomenon would require experimental verification of the linearity (or lack thereof) of the behavior.

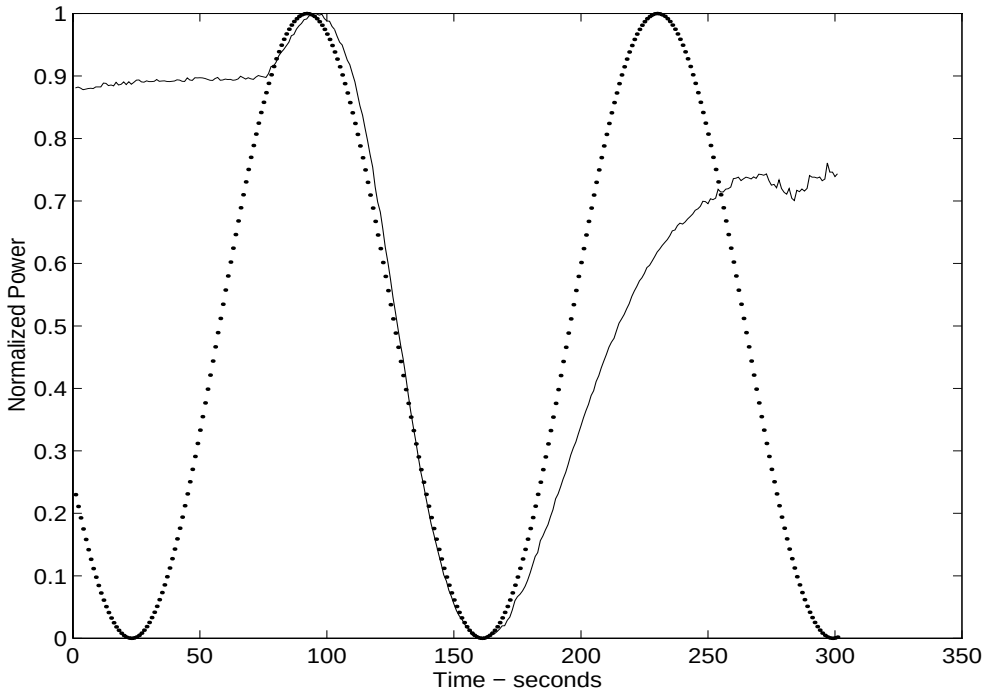

FIGURE 4.3-1 Theoretical and Measured Variation in the Normalized Coupled Power using the Gaussian Approximation.

As regards the step -index approximation, it is easy to see that there are around two or three orders of magnitude difference in the value of C predicted by the Gaussian approximation, and hence application of those results are questionable. The above arguments about the validity of the Gaussian model are further enhanced by a simple correlation analysis of the theoretical and practical data. The correlation coefficient has a value of 90.14% for the data shown in Fig. (4.3-1), which enables us to have statistical confidence in our model. This is true only if the regions where the deviation from the actual behavior due to the reasons detailed above is neglected from the analysis. If the regions where the deviant behavior is included, the correlation coefficient drops to 33.93%, but this is expected as the Mean Squared Error (MSE) is large for the initial part of the curve.

5 Conclusions

A novel technique for the design and analysis of single mode optical fiber couplers has been presented. While it is not possible at the present stage of experimental verification to state that the model is accurate enough for practical applications, the qualitative evaluation of the model seems to suggest that it shows promise. Future work needs to refine the numerical analysis to account for the variation of some of the other parameters like the effect of axial stress on the diffusion constant. These are issues that need to be addressed by a materials engineer. However, if it becomes possible to predict the time evolution of the coupling process to within the required accuracy, this will mean a significant reduction in the labor required to manufacture couplers. One issue that has not been examined in great detail is the wavelength dependence of such couplers. Promising results may be achieved insofar as the WDM capabilities of the couplers are concerned. The possibility of accurate index profiling on the coupling region would be of great benefit in further testing of the model.

6 References

[McL88] McLandrich, M.N., *Core Dopant Profiles in Weakly Fused Single Mode Fibers*, Electronics Letters, v. 24, no.3, 1988, pp. 8-10.

[Bot88] Botham, C.P, *Theory of Tapering Single Mode Optical Fibres by Controlled Core Diffusion*, Electronics Letters, v. 24, no. 4, 1988, pp. 243-244.

[Vup94] Vuppala, V.B., *Improvements in Fiber Optic Coupler Fabrication Techniques*, M.S. Thesis, VPI&SU, Sept. 1994.

[Bur88] Bures, J., et al, *Analyse d'un coupleur bidirectionnel a fibres optiques monomodes fusionnees*, Applied Optics, v.22, 1988 pp. 1918-1922.

[Pay85] Payne, F.P. et al, *Modeling Fused Single Mode Fibre Couplers*, Electronics Letters, v. 21, no. 11, 1985, pp. 461-462.

[Sny83] Snyder, A.W. and Love, J.D., *Optical Waveguide Theory*, Chapman and Hall, London, 1983.

[Cra75] Crank, J., *The Mathematics of Diffusion*, Clarendon Press, Oxford, 1975.

[Abr70] Abramovitz, M., and Stegun, I., *Handbook of Mathematical Functions*, Dover, NY, 1970.

[Car59] Carslaw, H.S. and Jaeger, J.C., *Conduction of Heat in Solids*, Oxford Univ. Press, NJ, 1959.

[Hau10] Haus, H.A. and Huang, W., *Coupled Mode Theory*, Proc. IEEE, v. 79, no. 10, pp. 1505-1518, 1991.

[Saf93] Safaii-Jazi, A., *EE5154 Optical Waveguide Theory -- Class Notes*, VPI&SU, Spring 1993.

[McI73] McIntyre, P.D., and Snyder A.W., *Power Transfer between Optical Fibers*, JOSA v. 63, no. 12, 1973.

[Sny81] Snyder, A.W., *Understanding Monomode Optical Fibres*, Proc. IEEE, v.69, pp. 6-

13, 1981.

[Gre87] Grewal, B.S., *Higher Engineering Mathematics*, Khanna Publishers, New Delhi, 1987.

[Mat70] Matthews, J., and Walker, R.L, *Mathematical Methods of Physics*, W.A. Benjamin, NY, 1970.

[Shi90] Shiraisi, K., et al, *Beam Expanding Fiber Using Thermal Diffusion of the Dopant*, IEEE JLT, v. 8, no. 8, 1990, pp. 1151-1161.

[Ada81] Adams, M.J., *An Introduction to Optical Waveguides*, John Wiley, NY, 1981.

[Lov87] Love, J.D., *Spot Size, Adiabaticity, and Diffraction in Tapered Fibres*, Electronics Letters, v.23, no. 19, 1987, pp. 993-994.

[Gun94] Gunther, M.F., *Personal Communication*, December 1994.

[Kra86] Krause, J. et al, *Splice Loss of Single-Mode Fiber as Related to Fusion Time, Temperature and Index Profile Alteration*, IEEE JLT, v. 4, 1986, pp. 837-840.

Vita

The author was born in Trivandrum, India on June 20, 1970. He received the BSEE from the College of Engineering, Trivandrum at the University of Kerala, in June 1991. After graduation, he was employed by the Center for Development of Telematics (CDOT), Bangalore, India, as a systems engineer in the field of digital switching. He joined the graduate program at Virginia Tech in the fall of 1992, where he was a research assistant at the Fiber and Electro-Optics Research Center (FEORC).

After defending his thesis, Mr. Velayudhan was employed by LCC Incorporated at Arlington, VA. At present, he is employed by Qualcomm Incorporated, San Diego, CA. His main interests are in RF propagation, CDMA network engineering, and communication system design.